Queuosine biosynthetic enzyme, QueE moonlights as a cell division regulator

Samuel A. Adeleye[1], Srujana S. Yadavalli[1]*

[1]Waksman Institute of Microbiology and Department of Genetics, Rutgers University, Piscataway NJ 08854

*Corresponding author

Waksman Institute of Microbiology

Rutgers University

190 Frelinghuysen Rd

Piscataway NJ 08854

Phone: 848-445-0251

Email: sam.yadavalli@rutgers.edu

Short title: Queuosine biosynthetic enzyme and its moonlighting function

Keywords: Queuosine, tRNA modification, cell division, bacteria, stress response, moonlighting protein

Abstract

In many organisms, stress responses to adverse environments can trigger secondary functions of certain proteins by altering protein levels, localization, activity, or interaction partners. *Escherichia coli* cells respond to the presence of specific cationic antimicrobial peptides by strongly activating the PhoQ/PhoP two-component signaling system, which regulates genes important for growth under this stress. As part of this pathway, a biosynthetic enzyme called

QueE, which catalyzes a step in the formation of queuosine (Q) tRNA modification is upregulated. When cellular QueE levels are high, it co-localizes with the central cell division protein FtsZ at the septal site, blocking division and resulting in filamentous growth. Here we show that QueE affects cell size in a dose-dependent manner. Using alanine scanning mutagenesis of amino acids in the catalytic active site, we pinpoint particular residues in QueE that contribute distinctly to each of its functions – Q biosynthesis or regulation of cell division, establishing QueE as a moonlighting protein. We further show that QueE orthologs from enterobacteria like *Salmonella typhimurium* and *Klebsiella pneumoniae* also cause filamentation in these organisms, but the more distant counterparts from *Pseudomonas aeruginosa* and *Bacillus subtilis* lack this ability. By comparative analysis of *E. coli* QueE with distant orthologs, we elucidate a unique region in this protein that is responsible for QueE's secondary function as a cell division regulator. A dual-function protein like QueE is an exception to the conventional model of "one gene, one enzyme, one function", which has divergent roles across a range of fundamental cellular processes including RNA modification and translation to cell division and stress response.

Author Summary

In stressful environments, proteins in many organisms can take on extra roles. When *Escherichia coli* bacteria are exposed to antimicrobial compounds, the cell activates the PhoQ/PhoP signaling system, increasing the production of an enzyme called QueE. QueE is usually involved in the formation of queuosine (Q) tRNA modification. When cells make abundant QueE, it interacts with a vital division protein, FtsZ, disrupting division and causing elongation − a "moonlighting" function. Detailed study of QueE reveals specific regions involved in Q biosynthesis or cell division. QueE in organisms closely related to *E. coli* also has dual roles, while distant relatives are unifunctional. Comparative analysis identifies a unique *E. coli*

QueE region regulating cell division. This study shows QueE's versatility in linking and impacting distinct cellular processes such as RNA metabolism, protein translation, cell division, and stress response.

Introduction

Moonlighting proteins are multifunctional molecules that challenge the one-gene-one-function paradigm [1,2]. They are prevalent across all kingdoms of life, from humans to bacteria. In bacteria, they have been shown to link vital metabolic processes to physiological stress responses such as regulation of cell size [3], adhesion [4], bacterial virulence, and pathogenicity [5,6]. Moonlighting proteins associated with cell division are particularly intriguing because they connect this fundamental process to many additional networks that can profoundly influence cellular physiology. Specific examples include glucosyltransferases – OpgH in *Escherichia coli* and UgtP in *Bacillus subtilis*, which modulate cell division based on nutrient availability [3,7,8]. In *E. coli*, DnaA, known for its role in initiating DNA replication, also acts as a transcription factor regulating gene expression [7]. In *B. subtilis*, protein DivIVA has been implicated in chromosome segregation and spore formation apart from its role in cell division [9]. Studying moonlighting proteins provides a fascinating path to understanding protein functionality, interactions, and complexity within a cell. While our understanding of moonlighting proteins in bacteria has advanced significantly in recent years, several knowledge gaps and challenges remain in this field of research. One of the primary knowledge gaps is the precise molecular mechanisms underlying moonlighting. While some moonlighting functions have been identified and characterized, we often lack a comprehensive understanding of how a single protein can perform multiple functions.

Our previous work found that an enzyme – QueE – involved in the biosynthetic pathway for queuosine (Q) tRNA modification also plays a role in stress response [10]. Q is a hypermodified guanosine that is found ubiquitously at the wobble position of the anticodon loop of specific tRNAs – $tRNA^{His}$, $tRNA^{Tyr}$, $tRNA^{Asp}$, and $tRNA^{Asn}$ [11–14]. Q-tRNA modification is crucial to maintain translation fidelity and efficiency [15]. It has also been implicated in redox, virulence, development, and cancers [14,16,17]. Despite its universal distribution and importance, only bacteria are capable of *de novo* synthesis of Q from guanosine triphosphate (GTP), and eukaryotes salvage precursors of Q from diet or gut bacteria [11,14]. In the biosynthesis of Q, three enzymes QueD, QueE, and QueC, are required to produce a vital intermediate $PreQ_0$ [18]. Specifically, QueE (also called 7-carboxy-7-deazaguanine or CDG synthase) catalyzes the conversion of the substrate CPH_4 (6-carboxy-5,6,7,8-tetrahydropterin) to CDG (7-carboxy-7-deazaguanine) [19,20]. The role of QueE in the biosynthesis of Q has been well characterized, and crystal structures of QueE homologs from *Bacillus subtilis*, *Burkholderia multivorans*, and *Escherichia coli* have been solved, providing insights into the catalytic mechanism [19–22]. More recently, a second function for QueE has been described during the stress response of *E. coli* cells exposed to sub-MIC levels of cationic-antimicrobial peptides (AMP) [10]. During this response, the PhoQ/PhoP two-component signaling system, which plays an important role in sensing antimicrobial peptides and several other signals [23–25] is strongly activated, leading to an increase in QueE expression (Fig 1a). When QueE is upregulated in the cell, it binds at the site of cell division and blocks septation. Consequently, *E. coli* cells grow as long heterogeneous filaments ranging from a few microns to hundreds of microns in length. It has been shown that QueE localizes to the septal Z-ring, a vital structure in bacterial cell division [26,27], inhibiting septation post-Z ring formation in an SOS-independent manner [10]. This QueE-mediated filamentation phenotype is also observed under other conditions that activate the PhoQ/PhoP system robustly, such as when cells lacking MgrB (a negative feedback inhibitor

of PhoQ [28,29]) are grown under magnesium limitation. Although historically filamentation was considered a sign of death, it can also be a crucial adaptive response to stress [30–33].

In this study, using QueE as a model, we investigate the molecular determinants that allow a protein to perform two distinct functions. We analyze QueE's dual roles in tRNA modification and cell division by utilizing a specialized northern blotting technique and microscopy, respectively, as readouts. By examining single alanine mutants and variants of *E. coli* QueE (*Ec*QueE), we establish that the catalytic activity required for QueE's biosynthetic role is dispensable for its function as a cell division regulator. As a corollary, we identify several individual amino acid residues and a specific region in *Ec*QueE, which are necessary to cause filamentation but not for Q biosynthesis. Analysis of QueE homologs from different bacteria shows that the moonlighting functions of QueE are conserved among other enterobacteria, suggesting this mode of cell division regulation is widespread.

Results

Increased expression of QueE leads to its secondary activity in *E. coli* cell division.

To study the molecular determinants in QueE contributing to its dual functions, we utilize two distinct readouts (Fig 1b). Firstly, to test QueE's function in the formation of Q modification, we adapted published methods based on a specialized gel containing N-acryloyl-3-aminophenylboronic acid (APB) and northern blotting to detect queuosinylated tRNAs (Q-tRNAs) [35,36]. In this technique (APB gel and northern blotting), modified Q-tRNAs containing cis-diol reactive groups migrate slower than unmodified guanosinylated-tRNA (G-tRNAs) [36]. Secondly, to examine QueE's ability to cause filamentation, we use phase contrast microscopy and monitor cell morphology. Using Δ*queE* cells harboring *queE* on an IPTG-inducible plasmid, we analyzed Q-tRNA formation and filamentation in the presence or absence of the inducer.

Wild-type (WT) cells carrying an empty plasmid were included as a control. As a positive control, WT cells show the formation of Q-tRNA^{Tyr} (Fig 1c). As expected, Δ*queE* cells carrying an empty vector show a band corresponding to unmodified guanosinylated-tRNA^{Tyr} (G-tRNA^{Tyr}) but not queuosinylated-tRNA^{Tyr} (Q-tRNA^{Tyr}), confirming that QueE is required to produce Q. The complementation of Δ*queE* cells with WT QueE restores the formation of intact Q-tRNA^{Tyr} regardless of induction, indicating that the overexpression of the enzyme is not necessary for the complementation of Q-tRNA synthesis activity. Regarding cell morphology, cells lacking QueE do not filament. Δ*queE* cells expressing basal levels of QueE in the absence of inducer also do not filament, however, Δ*queE* cells induced to express WT QueE show filamentation (Fig 1d,[10]), implying that increased expression of QueE is needed for cell division inhibition.

QueE regulates cell length in a dose-dependent manner.

Expression of *queE* is upregulated during filamentation of *E. coli* cells in response to sub-lethal concentrations of a cationic antimicrobial peptide, C18G [10]. These elongated cells vary from ~2 to hundreds of microns in length, with an average size of ~20 µm. Interestingly, *queE* expression from an IPTG-inducible promoter on a plasmid in wild-type (WT) cells also causes filamentation. To systematically examine the effect of increasing QueE expression on cell length, we performed an IPTG titration using the inducible plasmid encoding *E. coli* QueE (*Ec*QueE) in MG1655 Δ*lacZYA* cells. As the IPTG concentration is increased from 0 to 500 µM, we observe a significant increase in the mean cell length, ranging from approximately 3 to 25 µm, respectively (Fig 2). The average cell length obtained for uninduced cells carrying *queE* on a plasmid is similar to that of the cells containing an empty vector. This indicates that any leaky expression of *queE* encoded by the plasmid has a negligible impact on the cell length. The average cell lengths of 18-25 µm obtained for 250-500 µM of IPTG are comparable to those observed for WT cells grown in the presence of sub-MIC level of cationic antimicrobial peptide or Δ*mgrB* cells starved for Mg^{2+} [10], suggesting that overexpression of QueE on a plasmid is a

good proxy for upregulation of this enzyme under strong PhoQP-activating stress conditions. It is to be noted that the average cell lengths at higher levels of induction are likely underestimated due to the technical limitations in fitting some of the long filaments into the imaging window during microscopy. Overall, our data show a gradual and linear increase in the extent of filamentation with induction. To confirm if higher induction indeed results in increased levels of QueE protein in cells, we cloned and expressed a His_6-tagged *Ec*QueE on an IPTG-inducible plasmid. This construct behaves similarly to our untagged QueE in causing filamentation upon induction and allows us to monitor His_6-*Ec*QueE levels at different inducer concentrations (Fig S1a-b). Consistent with our expectation, higher IPTG concentrations correlate with higher amounts of His_6-*Ec*QueE in cells as visualized by western blotting (Fig S1c-d), and average cell lengths correlate with QueE abundance (Fig S1f). As an added control, we show that the His_6-*Ec*QueE maintains the biosynthetic activity to produce Q-tRNAs (Fig S1e). Together, our data indicate that QueE levels need to be about 3-fold or higher than basal (uninduced) expression level to cause cell elongation by greater than 2-fold. Induction with IPTG at 250-500 µM (average cell lengths ranging from 18-25 µm) leads to an estimated 7 to 8-fold increase in QueE levels. In filaments produced under PhoQP activation conditions (WT cells grown in the presence of sub-MIC level of cationic antimicrobial peptide or Δ*mgrB* cells starved for Mg^{2+} [10],), the cell lengths obtained are comparable to plasmid overexpression, where the QueE levels would be upregulated by ~7 fold. Collectively, these results show that QueE levels modulate cell division frequency in a dose-dependent manner.

QueE's function in queuosine-tRNA biosynthesis is independent of its role as a cell division regulator.

Previous genetic analysis has shown that the cellular filamentation phenotype observed during the stress response is QueE-dependent but independent of the other components involved in Q synthesis [10]. We wondered if QueE's role in regulating cell division is functionally linked to its

activity as a Q biosynthetic enzyme. In other words, does the catalytic active site of QueE contribute to its ability to inhibit septation? To answer this question, we selected amino acid residues in *Ec*QueE vital for Q synthesis based on the crystal structure [20] and performed alanine scanning mutagenesis (Fig 3a-b). Amino acids Q13, E15, and R27 participate in substrate binding, three Cys residues – C31, C35, and C38 bind iron-sulfur clusters, T40 binds magnesium, and residues G94, S136, and Q189 are predicted to be involved in cofactor (S-adenosyl methionine) binding [19,20]. We also included in our analysis three lysine residues identified to be acetylation sites in *Ec*QueE – K60, K66, and K194 as lysine acetylation may affect protein activity [36–39].

We cloned the selected single alanine mutants of QueE on an IPTG-inducible plasmid and expressed each variant in a Δ*queE* background. We then analyzed the effect of each mutant on Q-tRNA production and cell morphology using APB gel-northern blotting [35,36] and microscopy, respectively (Fig 3, S2). Notably, mutations at several positions believed to be important for catalysis (Q13, T40, G94, S136, and Q189) and acetylation of QueE (K60 and K194) have a negligible effect on either function (Fig S2). While an individual mutation may affect the catalytic speed or efficiency of QueE, in this study, we are interested in the overall effect of a mutation in QueE on the formation of the end product (modified Q-tRNA) as a proxy for a functional biosynthetic enzyme. Therefore, these mutations were not considered for further analysis.

Interestingly, one of the mutants, QueE R27A, abolished Q-tRNA formation but retained the ability to cause filamentation like the WT (Fig 3c-d, S2). The C38A mutation also prevents Q-tRNA formation, however, expression of this mutant does not lead to filamentation, suggesting that the mutation may disrupt overall protein structure and stability. To further characterize the cellular localization of the R27A mutant, we created an N-terminally-tagged YFP-QueE-R27A

fusion. The YFP-QueE-WT clone behaves similarly to the untagged protein in modulating septation [10] and is functional in Q-biosynthesis (Fig S2d). The R27A construct localizes to the Z-ring similarly to the localization of the WT (Fig 4a,[10]). In addition, the mean length of the filamenting cells observed for the R27A mutant is comparable to that of WT, even though the fluorescence signal for the R27A mutant suggests a somewhat lower level of its expression relative to the WT (Fig 4c-d). QueE-mediated filamentation also occurs when cells lacking MgrB – a negative feedback inhibitor of PhoQ) – are grown in low magnesium conditions [10]. Consistent with our expectation, the QueE-R27A mutant mimics the WT QueE in restoring filamentation in a Δ*mgrB* Δ*queE* strain (Fig 4b).

In contrast to the R27A mutant, we identified four mutants, E15A, C31A, C35A, and K66A, which do not affect Q-tRNA synthesis but selectively impair the ability to inhibit septation. To cause a block in cell division, QueE needs to be expressed at high levels (≥ 3X basal levels), so it is possible that these mutants suppressing filamentation are expressed at levels insufficient to hinder division. To determine the expression levels of these individual mutants, we measured fluorescence by incorporating each mutation into the YFP-tagged QueE background. YFP-QueE-E15A and YFP-QueE-K66A show very low fluorescence, indicating that these mutations affect protein stability. Both mutants, YFP-QueE-C31A and YFP-QueE-C35A, display fluorescence at a level comparable to or higher than YFP-QueE-WT, indicating that the lack of filamentation in strains expressing these mutants is not due to a lower amount of protein in cells (Fig S2c). In addition, we performed western blotting to confirm that the proteins YFP-QueE-C31A and YFP-QueE-C35A are produced at full-length at levels comparable to that of WT (Fig S3). It is important to note that IPTG induction and QueE overexpression are not required for Q-tRNA synthesis (Fig 1c), therefore we tested the possibility that the C31A and C35A variants may be catalytically less active than wild-type QueE by performing APB-northern blots for cells expressing these variants with or without induction. QueE-C31A and QueE-C35A showed Q-

tRNA^{Tyr} formation even in the absence of induction (Fig S4), indicating that these mutants are fully active in Q-tRNA synthesis. In conclusion, we have identified and described single amino acid residues in *Ec*QueE that specifically affect either its function in Q-tRNA biosynthesis or cell division. Together, our results establish that the role of QueE as a modulator of septation is independent of its function in the Q-biosynthetic pathway.

Dual functions of QueE are conserved among *E. coli* and related bacteria.

Consistent with the fact that *de novo* biosynthesis of Q is a characteristic of most prokaryotes [40], QueE is widely conserved among bacteria [14,40,41]. Although the role of *E. coli* QueE (*Ec*QueE) in Q biosynthesis is well established [20], the homolog from *Bacillus subtilis* (*Bs*QueE) was the first to be characterized in terms of its biochemical properties and detailed catalytic mechanism [18,19,42]. Intriguingly, these two enzymes are less than 40% similar([10,20], Fig S5). Accordingly, QueE homologs across bacterial genera appear to be highly divergent in terms of their gene and protein sequences, resulting in distinct clusters based on sequence similarity analysis [20]. QueE protein sequences are increasingly dissimilar as we move farther from enterobacteriaceae within bacterial phylogeny. Therefore, we hypothesized that the sequence divergence among QueE orthologs may impact their functions in Q-tRNA biosynthesis and/or regulation of cell division. To test this hypothesis, we selected and analyzed orthologs of QueE from other gamma proteobacteria – *Klebsiella pneumoniae* (*Kp*QueE), *Salmonella Typhimurium* (StQueE), *Pseudomonas aeruginosa* (*Pa*QueE), and a firmicute, *Bacillus subtilis* (BsQueE). Based on the multiple sequence alignment of selected QueE orthologs and the corresponding phylogenetic tree (Fig S5), as expected *Bs*QueE is the most distant ortholog, followed by *Pa*QueE.

To test the ability of each QueE ortholog to synthesize Q-tRNAs and inhibit cell division, we cloned each gene into an IPTG inducible multicopy plasmid and induced expression in *E. coli*

Δ*queE* cells. All of the QueE orthologs tested here are functional in producing tRNAs modified with Q (Fig 5a), indicating that this function is well-conserved among these orthologs. However, when we observe the morphology of cells expressing these orthologs, interestingly, only *Kp*QueE and *St*QueE trigger inhibition of septation, but *Bs*QueE and *Pa*QueE do not, when expressed in *E. coli* Δ*queE* cells (Fig 5b). We considered the possibility that heterologous expression of *Bs*QueE and *Pa*QueE may affect their folding and stability. So, we analyzed the expression of these two QueE orthologs using the YFP-tagged protein fusions along with *Ec*QueE as a control. Upon expression, both YFP-*Bs*QueE and YFP-*Pa*QueE show similar levels of fluorescence as that of YFP-*Ec*QueE (Fig 5c) and we confirmed that the proteins YFP-*Bs*QueE and YFP-*Pa*QueE are produced at full length at levels comparable to that of YFP-*Ec*QueE by western blotting (Fig S3).

While the expression of orthologous proteins in *E. coli* is convenient, it is not testing their function in the native environment where additional factors, which may help cause filamentation, are missing. To test this scenario, we expressed each QueE ortholog on a plasmid in its original host, i.e., *Kp*QueE in *K. pneumoniae*, *Pa*QueE in *P. aeruginosa* cells, and so on. For stable expression of *Bs*QueE in *B. subtilis*, we prepared a genomic construct carrying an IPTG-inducible *Bs*QueE at the *amyE* locus (details in the methods section). As observed for expression in *E. coli*, *Kp*QueE and *St*QueE cause filamentation in their corresponding host cells, however, *Bs*QueE and *Pa*QueE fail to do so (Fig S6). The average cell lengths for *P. aeruginosa* cells expressing *Pa*QueE were similar to that of control cells carrying an empty vector (Fig S6b). Notably, *B. subtilis* cells show cell elongation and/or chaining to varying extents irrespective of QueE expression but there is no change in average cell lengths with increased QueE expression. However, there is still a possibility that partial or complete septa may be formed between cells within a chain of *B. subtilis* cells expressing *Bs*QueE. We stained the cytoplasmic membrane with the FM4-64 dye to visualize any additional invaginations or

septa *B. subtilis* cells expressing *Bs*QueE vs. control cells that do not express this protein. We did not observe significant differences in septa formed between the two cell types, indicating that *Bs*QueE may not impact cell division in *B. subtilis* (Fig S6c). To ensure that there is no problem with overexpression of either *Pa*QueE or *Bs*QueE in their respective hosts, we generated YFP-tagged versions of these proteins and measured YFP fluorescence as a function of their level of expression with and without induction. Both YFP-*Pa*QueE and YFP-*Bs*QueE show a robust increase in YFP fluorescence upon induction, and we confirmed the corresponding expression of the full-length protein by western blotting (Fig S6d-e). There were no bands observed for uninduced samples, suggesting a tight regulation of protein expression in these constructs. Despite the strong induction and expression of *Bs*QueE in *B. subtilis* and *Pa*QueE in *P. aeruginosa* the impact on cell division, if any, seems negligible. Taken together, these results show that the ability of QueE to disrupt cell division is specific to enterobacterial counterparts, closely related to that of *E. coli*.

A distinct region (E45-E51) in *E. coli* QueE is dispensable for its role in queuosine-tRNA biosynthesis but not for the regulation of septation.

Besides sequence variation, the QueE enzyme family also displays a high degree of structural divergence [20], suggesting a molecular basis for the differences observed in the ability of QueE orthologs to regulate cell division. Among the selected QueE proteins, *Bs*QueE and *Pa*QueE do not cause filamentation. *Bs*QueE and *Pa*QueE protein sequences share an identity of only ~19%, 24%, respectively, and <40% similarity with *Ec*QueE (based on EMBOSS Needle pairwise sequence alignments [43], yet they are catalytically active in Q-tRNA synthesis (Fig 5, S6). To gain insights into the mechanism, we generated a structural alignment to compare the structures of *Ec*QueE[20], *Bs*QueE[19], and an AlphaFold [44,45] model of *Pa*QueE (Fig 6a). We see that the catalytic core region corresponding to QueE's CDG synthase activity is preserved between the three QueE proteins despite low sequence similarity Fig 6,[20].

Unsurprisingly, amino acid residues involved in substrate and co-factor binding are well-conserved in the orthologs (Fig. S5a). Based on the structural alignment, we noted a distinguishing feature of *Ec*QueE in the region spanning 22 amino acids E45 through W67 (Fig 6). According to the *Ec*QueE crystal structure, this region comprises two helical motifs – αT2 and α2', connected to each other and the rest of QueE *via* flexible loops [20]. This E45-W67 region from *Ec*QueE appears to be variable among other orthologs, where it is truncated or almost entirely missing in *Bs*QueE and *Pa*QueE (Fig. 6a). We hypothesized that this region with the two helices unique to *Ec*QueE contributes to its second function in inhibiting septation yet dispensable for its Q-biosynthetic function. To test this idea, we cloned *Ec*QueE variants lacking regions comprising either of the helices αT2 (ΔE45-E51), α2' (ΔV52-W67), or both (ΔE45-W67) and expressed them in Δ*queE* cells. Remarkably, *Ec*QueE mutants carrying deletions of either αT2, α2', or the entire region E45-W67 are functional in Q-tRNA production (Fig 6b), indicating that the E45-W67 region is dispensable for Q biosynthesis. To check if the deletion mutants are catalytically less active than the WT in Q-tRNA synthesis, we performed APB-northern blotting for cells expressing these deletion mutants with or without induction. We noticed that the *Ec*QueE ΔE45-E51 mutant is fully functional in forming Q-tRNA^{Tyr} in cells that are uninduced or induced with IPTG (Fig 6b, S7). The other two deletions (ΔV52-W67 and ΔE45-W67) do not show significant Q-tRNA^{Tyr} in the absence of induction. When the cells are induced with IPTG both these mutants form Q-tRNA^{Tyr} albeit to a lower extent relative to the *Ec*QueE ΔE45-E51 mutant and the WT, suggesting that the ΔV52-W67 and ΔE45-W67 mutants are catalytically weaker than the WT. It is notable the ΔV52-W67 mutant only has a slight reduction in Q-tRNA formation and the ΔE45-W67 mutant still retains the ability to form Q-tRNA upon overexpression (Fig 6b, S7), a condition that mimics PhoQP-activating stress where QueE is upregulated. Then, we observed the cell morphology and none of the deletion constructs caused filamentation (Fig 6c), supporting our hypothesis that the E45-W67 region mediates QueE's role in cell division regulation. To control for the possibility that the deletion of this region affects overall protein

stability and level in the cell, we quantified protein levels using a YFP-QueE-ΔE45-W67 construct by monitoring cell fluorescence. We see that the level of fluorescence for YFP-QueE-ΔE45-W67 is comparable to that of WT (Fig 6d) and we confirmed that the full-length protein YFP-QueE-ΔE45-W67 is produced at levels comparable to that of YFP-QueE WT by western blotting (Fig S3).

Given the ability to cause filamentation by *St*QueE and *Kp*QueE, closely related orthologs to *Ec*QueE, we wondered if there is a consensus sequence that can predict whether a given QueE sequence may confer an ability to inhibit cell division. We identify several conserved residues using bioinformatic analysis of QueE protein sequences from 18 representative enterobacteria (Fig S8). To better represent the amino acid diversity at each position, we generated a WebLogo [46] corresponding to the E45-W67 region in *Ec*QueE, revealing significant features of this sequence (Fig 7). In particular, amino acids Glu or Asp at position 45, Ile or Val at position 57, Lys60, Thr61, Glu or Asp at position 63 and Trp67 (based on *Ec*QueE numbering) are highly conserved suggesting that their occurrence correlates with QueE's ability to impair septation.

Discussion

Moonlighting proteins highlight the versatility and adaptability of bacterial proteins [1,2]. Studying these multifunctional proteins in a model organism such as *E. coli* provides a deeper understanding of protein functionality. Bacterial cell division is a complex process orchestrated primarily by the essential proteins that form the divisome, with FtsZ being one of the most central and well-studied [26,27,47–51]. However, in addition to these core proteins, there are non-essential, auxiliary proteins that, while not strictly required for cell division, play supportive roles in regulating the process. A notable example is SulA, an inhibitor of FtsZ polymerization induced in response to DNA damage to temporarily halt cell division [49,52–54]. Accessory

proteins, SlmA and Noc, ensure division occurs at appropriate sites and not over the chromosome [55–58]. These and several other auxiliary proteins, while "non-essential", can be crucial for survival to fine-tune and ensure optimal cell division under a variety of conditions in natural environments [59–61].

The enzyme QueE, known for its role in Q biosynthesis [62], also regulates septation [10]. While QueE-dependent filamentation is not linked to the Q-biosynthetic pathway, it was unclear how QueE performs these two unrelated functions. Here, we show that the regulation of cell size is dependent on the levels of QueE. We find that as QueE expression increases, the average cell length also increases. Using site-directed mutagenesis of catalytically important amino acid residues in *Ec*QueE [20], we identify specific residues that selectively affect filamentation or Q-biosynthesis. In particular, the QueE-R27A mutant is catalytically dead for Q-biosynthesis yet modulates septation. Like the WT, QueE-R27A localizes with FtsZ and the Z-ring, indicating that the septal localization is still maintained in this mutant that is catalytically inactive for Q-biosynthesis. Thus, QueE's role in queuosine biosynthesis and modulation of cell division are not functionally linked, elucidating QueE as a moonlighting protein (Fig 7).

Based on the structural alignment of QueE orthologs, we observe that the catalytic core domain required for Q biosynthesis is well-preserved (Fig 6,[20]) and the expression of different QueE enzymes in an *E. coli ⊿queE* strain restores Q-tRNA synthesis (Fig 5). However, some peripheral structural elements, especially the regions surrounding the iron-sulfur cluster binding pocket, show remarkable variation among members of the QueE family ([20] Fig 6, S5a). Our results are consistent with the previous analysis that the sequence and structural diversity among QueE proteins do not impact its catalytic function or cofactor binding. Interestingly, Grell et al., ponder over the significance of such large variation in QueE structures. They show that differences in surface elements of QueE as a radical SAM enzyme are at least in part a likely

outcome of co-evolution with the cognate flavodoxin that allows for efficient protein-protein interactions [20]. Here, we note a stark variation in the region encompassing the two helices α2' and αT2 based on our structural comparison of *Ec*QueE, *Bs*QueE and *Pa*QueE (AlphaFold-generated model). We propose these variable features may explain whether or not a given QueE protein has a moonlighting function in modulating cell division. A particular region of interest – comprising E45 through W67 is distinctive to *Ec*QueE, and a sub-region E45 through E51 (αT2) is dispensable for Q biosynthesis but required to cause filamentation (Fig 6). Specific amino acids in this region are highly conserved among enterobacterial genera (Fig 7) and potentially mediate the interactions between QueE and proteins at the Z-ring during cell division. We demonstrate that in bacteria from at least three distinct genera, elevated expression of the native QueE ortholog leads to filamentous cell growth (Fig 5). This indicates that such a mechanism for cell division regulation is widely conserved among Enterobacteriaceae. Two other distant homologs from *P. aeruginosa* and *B. subtilis*, exhibiting lower sequence and structural similarity to *Ec*QueE than enterobacterial orthologs, do not show functional conservation in regulating septation. It is tempting to speculate that the lack of cell division regulation is primarily due to the sequence and structural differences between the QueE orthologs. If this is the case, it would be interesting to see if *Ec*QueE expression in *P. aeruginosa* can cause filamentation. To test this idea, we expressed *Ec*QueE on a shuttle vector in both *E. coli* and *P. aeruginosa*. Interestingly, we do not see any filamentation in *P. aeruginosa* but our control *E. coli* cells displayed filaments (Fig S9), indicating that there are likely additional factors and variations in cell division machinery in Pseudomonas and Bacillus involved in modulating cell division. The target(s) that QueE binds to and the mechanism by which it controls septation in *E. coli* are subjects of an ongoing inquiry.

Overall, bacteria possess diverse, species-specific regulators that modulate physiological responses based on environmental conditions or the cell's metabolic state. QueE serves as an example to underscore the intricate ways in which bacteria have evolved to use proteins in multiple roles, ensuring efficient coordination between processes like cell division and other essential cellular functions.

Materials and methods

Strains and plasmids

Details of the strains, plasmids, and oligonucleotides used in this study are provided in the supporting information (Tables A-C). *E. coli* K-12 MG1655 strain and its derivatives, plasmid pEB52, and its derivatives were gifts from Dr. Mark Goulian (University of Pennsylvania). The following strains, *Pseudomonas aeruginosa* PA01, *Klebsiella pneumoniae* ATCC 13883, *Bacillus subtilis* 168, *Bacillus subtilis* IS75, and *S. Typhimurium* 14208, were gifts from Drs. Bryce Nickels (Rutgers), Huizhou Fan (Rutgers), Jeffrey Boyd (Rutgers), David Dubnau (Rutgers), and Deiter Schifferli (University of Pennsylvania); plasmids pEG4 and pPSV38 were gifts from Drs. Kenn Gerdes (Copenhagen) and Simon Dove (Boston Children's Hospital, Harvard Medical School), respectively.

Cloning of QueE and its variants

Plasmids encoding single alanine mutants of *E. coli* QueE, His_6-QueE, and YFP-QueE were made using inverse PCR or single primer methods using pRL03 (untagged QueE), pSY85 (His_6-QueE) or pSY76 (YFP-QueE) as templates. All the plasmids used to test QueE expression in *E. coli* are derivatives of pTrc99a [63]. pTrc plasmids are IPTG-inducible and considered medium copy with a copy number of ~30 per cell and they carry *lacI*^{q}, which represses the lac promoter reducing leaky expression. QueE orthologs from *S. Typhimurium* 14028 and *Pseudomonas*

aeruginosa PA01 were cloned using restriction sites, EcoRI and BamHI, while *Bacillus subtilis* QueE was cloned using the SacI and BamHI restriction sites in a pEB52 vector resulting in the plasmids pSA21, pSA22, and pSY45 respectively. Since *K. pneumoniae* ATCC 13883 has an intrinsic resistance to ampicillin/carbenicillin, the QueE gene from *K. pneumoniae* was cloned into a pBAD33 vector using the Xba1 and Kpn1 restriction sites to create plasmid pSA59. We also added a ribosome binding site (RBS) to pBAD33, upstream of the start site of the cloned gene using the inverse PCR cloning method. Plasmids pSA60, pSA61, and pSA62 encoding variants of *E. coli* QueE, QueE-ΔE45-E51, QueE-ΔV52-W67, and QueE-ΔE45-W67 were made using inverse PCR. YFP-tagged QueE variants (pSA57-58, pSA73, pSA75-76, pSA119) were created by inverse PCR method, YFP-*Bs*QueE (pSA121) and YFP-*Pa*QueE (pSA126) for expression in *E. coli* were made using the NEB Hi-Fi Assembly protocol by substituting *Ec*QueE in the pSY76 background. Plasmid pSY76 (described in [10]) is a pTrc99a derivative containing a strong RBS (AAAGAGGAGA) at an optimal distance of 8 bp upstream of *yfp-queE*, which does not require the addition of IPTG for overexpression in *E. coli*. To prepare plasmid constructs for expression in *P. aeruginosa*, we used the shuttle vector pSV38 [64]. *Pa*QueE, YFP-*Pa*QueE, and *Ec*QueE were amplified from pSA151, pSA126, and pRL03, respectively, using the sequencing primers. The fragments were cloned into the pPSV38 vector using the Xba1 and EcoRI, and XbaI and HindIII, and EcoR1 and XbaI, cut sites to obtain pSA154, pSA156, and pSA157 respectively. Plasmids pSA154, pSA156, and pSA157 were transformed into *P. aeruginosa* PAO1 and selected on LB agar containing 30 µg mL^{-1} gentamycin, while pSA157 was transformed into *E. coli* MG1655 and selected on 15 µg mL^{-1} gentamycin. All constructs were confirmed by Sanger sequencing, and plasmids were transformed into chemically competent *E. coli* Top10 or XL1-Blue strains for maintenance in 20% glycerol at -80°C. Plasmids were transformed into MG1655 and its derivatives (TIM183, SAM31, or SAM96) as applicable.

Construction of *B. subtilis* strains encoding *Bs*QueE and YFP-*Bs*QueE

To generate genomic constructs encoding *Bs*QueE and YFP-*Bs*QueE in *B. subtilis*, YFP-tagged and untagged variants of *Bs*QueE were cloned into the pDR111 hyper-SPANK vector using the Sal1 and Nhe1 cut sites to obtain pSA149 and pSA147, respectively, empty vector was set as control. The ribosome binding site AAAGGAGAGGG corresponding to a well-expressed competence gene, *comGA* in *B. subtilis* [65,66] was included upstream of the *Bs*QueE and YFP-*Bs*QueE open reading frames. XL1-Blue cells were transformed with the ligation mixtures and selected using carbenicillin selection at 100 µg mL^{-1}. The resulting clones are pDR111 hyper-SPANK derivatives, incapable of replication in *B. subtilis* but carry front and back sequences of *amyE*, suitable for recombination into the *Bacillus subtilis amyE* locus. The constructs contain Phs, the hyper-SPANK promoter, which is IPTG-inducible. After confirming via Sanger sequencing, the plasmids were transformed into *B. subtilis* IS75 and selected for spectinomycin resistance (100 µg mL^{-1}). Colonies that grew were further screened for the absence of amylase activity. Briefly, the amylase test was done by inoculating colonies onto starch plates containing 100 µg mL^{-1} spectinomycin. After 8-12 hours of growth, when the plates were exposed to iodine, a halo zone around the colonies indicated a positive amylase activity. Strains that have undergone recombination (without the halo) are chosen for analysis, SAA50 (*B. subtilis* IS75 Δ*amyE*::pSA147 or *amyE::BsqueE*), SAA52 (*B. subtilis* IS75 Δ*amyE*::pSA149 or *amyE::yfp-BsqueE*), and SAA53 (*B. subtilis* IS75 Δ*amyE*::pPDR111 or *amyE::empty*).

Media, reagents, and growth conditions

Routine bacterial growth on solid agar was performed using LB Miller medium (IBI scientific) containing 1.5% bacteriological grade agar (VWR Lifesciences) at 37°C. Liquid cultures were grown at 37 °C with aeration in either LB miller medium or minimal A medium (MinA) (K_2HPO_4 (10.5 g l^{-1}), KH_2PO_4 (4.5 g l^{-1}), $(NH_4)_2SO_4$ (10.0 g l^{-1}), Na_3 citrate.$2H_2O$ (0.5 g l^{-1}), supplemented with 0.1% casamino acids, 0.2% glucose and 1 mM concentration of $MgSO_4$ unless otherwise

indicated. Throughout this study, MinA supplemented, as indicated above, will be referred to as supplemented MinA minimal medium. Antibiotics were used at final concentrations of 100 µg mL^{-1} (LB) or 50 µg mL^{-1} (minimal medium) for carbenicillin, 25 µg mL^{-1} for chloramphenicol, 100 µg mL^{-1} for spectinomycin, and 7.5 – 30 µg mL^{-1} for gentamycin as indicated. The *lac*/*trc* and *araBAD* promoters were induced using 500 µM b-isopropyl-D-thiogalactoside (IPTG) and 0.5% arabinose, respectively, unless otherwise specified.

For microscopy experiments, overnight cultures of strains harboring specified plasmids were grown in minimal medium (supplemented MinA as described above) and appropriate antibiotics, then back diluted (1:500) into fresh medium unless otherwise indicated. About 4-6 µL of cells were immobilized on glass slides containing agarose pads made from 1% agarose in 1X MinA salts. For the phase contrast microscopy, back-diluted cells were grown for 2 hours (OD_{600} ~0.2) and then induced for 3 hours with either 0.5 mM IPTG or 0.5% arabinose. Cells were grown under the same conditions to detect modified and unmodified tRNA using APB northern blotting. For the fluorescence microscopy and protein localization, SAM96 (*DqueE*) cells expressing either YFP-QueE (pSY76) or YFP-QueE-R27A (pSA58) and FtsZ-mCherry (pEG4) into SAM96 were grown for 4 hours, followed by addition of arabinose and growth for another 1 hour to reach OD_{600} ~0.4-0.5. To monitor single-cell fluorescence in cells expressing QueE and its variants, SAM96 cells containing plasmids (pSA57, pSA58, pSY76, pSA73, pSA75, pSA76, pSA119, pSA121, pSA126) were grown for 5 hours to reach OD_{600} 0.4-0.5. In fluorescence quantification experiments, the cultures were rapidly cooled in an ice slurry, and streptomycin was added at 250 µg mL^{-1} to halt translation. For IPTG titration experiments, overnight cultures of TIM183/pRL03 or TIM183/pSY85 and TIM183/pTra99a were back diluted (1:500) into fresh medium. These cells were grown for 2 hours and then induced with IPTG at concentrations 0, 10, 25, 50, 75, 100, 250, and 500 µM for 3 hours, followed by imaging.

For QueE expression in *P. aeruginosa*, overnight cultures of the *P. aeruginosa* carrying plasmids pSA154, pSA156, and pPSV38 were grown in LB containing 30 µg mL^{-1} gentamycin. *E. coli* cells containing pSA157 and pPSV38 were included as controls and grown in LB containing 15 µg mL^{-1} gentamycin. *P. aeruginosa* cultures were back diluted 1:500 in supplemented MinA containing 20 µg mL^{-1} gentamycin and induced with 2 mM IPTG for 6 hours. For *E. coli* cultures, 7.5 µg mL^{-1} gentamycin and 0.5 mM IPTG were used. 5 µl aliquots were used for microscopy, and the rest were pelleted for Coomassie staining and western blotting.

For QueE expression in *B. subtilis*, overnight cultures of strains SAA50, SAA52, and SAA53 were grown in supplemented MinA containing 100 µg mL^{-1} spectinomycin. The cultures were back diluted 1:500 in fresh medium and induced with 1 mM IPTG for 6 hours. 5 µl aliquots were used for microscopy and the rest were pelleted for Coomassie staining and western blotting. For cytoplasmic membrane staining with FM4-64, cells were grown in supplemented MinA containing 100 µg mL^{-1} spectinomycin and 1 mM IPTG for 5 hours and stained as described in the microscopy section.

Microscopy and image analysis

Phase contrast and fluorescence microscopy of MG1655 Δ*queE* (SAM96 or SAM31) cells harboring plasmids of QueE, single alanine mutants, QueE orthologs, and their variants were performed as previously described [10]. 4-6 µL of the cells were immobilized on 1% agarose pads, and their morphology was observed using a Nikon TiE fluorescent microscope with a TI2-S-HU attachable mechanical stage. The images were captured using a Teledyne Photometrics Prime 95B sCMOS camera with 1x1 binning. The Nikon Ti-E's perfect focus system (PFS) ensured continuous focus during imaging. YFP and mCherry fluorescent images were taken with a 100 ms exposure time at 20% intensity, while phase-contrast images were captured with a 40 ms exposure time and 20% intensity. All image acquisition during experiments was

managed using Metamorph software version 7.10.3.279. The background fluorescence was determined using the MG1655 Δ*queE* (SAM96) strain grown under the same conditions. The average cell fluorescence was quantified using ImageJ [67] and the MicrobeJ plugin [68]. Data from independent replicates was plotted using R. For FM4-64 staining, *B. subtilis* cells were treated with FM4-64 (Invitrogen) at a final concentration of 0.1 ug/ml, incubated in the dark for one hour followed by imaging using the mCherry channel.

APB gel electrophoresis and northern blotting

$tRNA^{Tyr}$ modified with queuosine (Q) in total cell RNA was detected using previously published protocols [35,36] with the following modifications. Total RNA was extracted from cell pellets using the Trizol RNA extraction method [69]. 150 ng of total RNA was deacylated in 100 mM Tris-HCl (pH 9.0) at 37°C for 30 minutes. The deacylated RNA was run on a 0.4 mm thick 7% Urea denaturing polyacrylamide gel, supplemented with 0.5% 3-acrylamidophenylboronic acid (APB). The RNA was transferred using a semi-dry system to a Nytran SuPerCharge nylon blotting membrane (VWR). After transfer, the membrane was crosslinked twice using a UV crosslinker (Fisher Scientific) at optimal conditions (254 nm wavelength and 1200 mJ energy) and hybridized in 50 mL hybridization buffer (750 mM NaCl and 75 mM sodium citrate, 20 mM Na_2HPO_4, 7% SDS, 0.04% BSA fraction V (high purity), 0.04% Ficoll 400, and 0.04% polyvinylpyrrolidone) at pH 7.0, supplemented with 200 µL sheared salmon sperm DNA (10 mg/mL). Following hybridization for 1 hour, $5'$-^{32}P labeled oligonucleotide (SA1, Table C in supporting information) with complementarity to $tRNA^{Tyr}$ were added and incubated for 16-18 hours at 50 °C. The blot was washed thoroughly with a low-stringent wash solution (450 mM NaCl and 45 mM sodium citrate, 25 mM Na_2HPO_4 (pH 7.2), 5% SDS, 0.2% BSA fraction V (high purity), 0.2% Ficoll 400, 0.2% polyvinylpyrrolidone, and DEPC ddH_2O) at 50°C for 15 minutes each, and once with stringent wash solution (150 mM NaCl and 15 mM sodium citrate, 1% SDS,

DEPC ddH_2O) at 50°C for 5 minutes. The blot was exposed to a phosphor imager screen and imaged using the phosphorimager (GE Amersham™ Typhoon) at a sensitivity of 4000.

Cell lysate preparation and western blotting

Cell pellets harvested from 25 mL cultures of TIM183/pSY85 grown in the absence or presence of varying concentrations of inducer (IPTG) were resuspended in 400 µL 20% sucrose/30 mM Tris pH 8.0. and 1 mL 3mM EDTA pH 7.2 was added. The cells were sonicated for ~30 sec (10-sec pulse, 10-sec gap, 3x) using a sonicator (Fisher Scientific, VCX-130 Vibra-Cell Ultrasonic). The resulting lysed cells were centrifuged at 600rpm for 5 minutes, and the supernatant was collected for further use. Each sample is normalized by the cellular biomass and loaded onto two 12% Bis tris gels using MES as a running buffer at 160V for 1 hour. One gel is stained using the Coomassie gel protocol, destained, and imaged using a Biorad Gel Doc XR+ System, while the other was processed for western blotting. Separated proteins were transferred to a PVDF membrane (Amersham™ Hybond™ P 0.2 µm) in a transfer buffer supplemented with 20% methanol. The His_6-QueE is detected with an anti-His primary antibody and IRDye-conjugated secondary antibody (LI-COR). The protein bands were visualized with the Odyssey CLx imaging system (LI-COR). To determine relative QueE abundance, band intensities were quantified using ImageJ [67] and normalized to the amount of protein in the uninduced sample.

Sequence and structural analysis

The protein sequences of QueE orthologs were obtained from Ecocyc [70]. Multiple sequence alignments were performed using Clustal Omega [71,72], and the phylogenetic tree diagrams were generated using Jalview [73]. The consensus sequence was generated using Weblogo [46,74]. The structural model of *Pa*QueE was computed using AlphaFold [44,45], and the structural alignment of *Bs*QueE, *Ec*QueE, and *Pa*QueE was generated using Pymol [75].

Acknowledgments

The authors would like to thank Drs. Mark Goulian, Bryce Nickels, Huizhou Fan, Dieter Schifferli, Jeffrey Boyd, David Dubnau, Simon Dove and Kenn Gerdes for generously sharing strains and plasmids. We are grateful to Drs. David Dubnau and Jeanette Hahn for sharing their expertise and helping us generate IPTG-inducible genomic constructs of *B. subtilis* expressing *B. subtilis* QueE. We thank the past and present members of the Yadavalli and Shah Labs for helpful discussions. We also thank Drs. Premal Shah, Manuela Roggiani, and Mark Goulian for critical reading of the manuscript. Srujana S. Yadavalli is supported by NIGMS R35 GM147566 and institutional start-up funds. Samuel A. Adeleye was supported by a Waksman Institute Busch Predoctoral Fellowship from 2020-22.

References

1. Singh N, Bhalla N. Moonlighting proteins. Annu Rev Genet. 2020;54: 265–285.
2. Jeffery CJ. An introduction to protein moonlighting. Biochem Soc Trans. 2014;42: 1679–1683.
3. Hill NS, Buske PJ, Shi Y, Levin PA. A moonlighting enzyme links Escherichia coli cell size with central metabolism. PLoS Genet. 2013;9: e1003663.
4. Jeffery C. Intracellular proteins moonlighting as bacterial adhesion factors. AIMS Microbiol. 2018;4: 362–376.
5. Henderson B. An overview of protein moonlighting in bacterial infection. Biochem Soc Trans. 2014;42: 1720–1727.
6. Henderson B, Martin A. Bacterial moonlighting proteins and bacterial virulence. Curr Top Microbiol Immunol. 2013;358: 155–213.
7. Levin PA, Angert ER. Small but mighty: Cell size and bacteria. Cold Spring Harb Perspect Biol. 2015;7: a019216.
8. Chien A-C, Zareh SKG, Wang YM, Levin PA. Changes in the oligomerization potential of the division inhibitor UgtP co-ordinate Bacillus subtilis cell size with nutrient availability. Mol Microbiol. 2012;86: 594–610.

9. Errington J. Regulation of endospore formation in Bacillus subtilis. Nat Rev Microbiol. 2003;1: 117–126.

10. Yadavalli SS, Carey JN, Leibman RS, Chen AI, Stern AM, Roggiani M, et al. Antimicrobial peptides trigger a division block in Escherichia coli through stimulation of a signalling system. Nat Commun. 2016;7: 12340.

11. Reader JS, Metzgar D, Schimmel P, de Crécy-Lagard V. Identification of four genes necessary for biosynthesis of the modified nucleoside queuosine. J Biol Chem. 2004;279: 6280–6285.

12. Kersten H, Kersten W. Chapter 2 Biosynthesis and Function of Queuine and Queuosine tRNAs. In: Gehrke CW, Kuo KCT, editors. Journal of Chromatography Library. Elsevier; 1990. pp. B69–B108.

13. Nishimura S. Structure, biosynthesis, and function of queuosine in transfer RNA. Prog Nucleic Acid Res Mol Biol. 1983;28: 49–73.

14. Vinayak M, Pathak C. Queuosine modification of tRNA: its divergent role in cellular machinery. Biosci Rep. 2009;30: 135–148.

15. Müller M, Legrand C, Tuorto F, Kelly VP, Atlasi Y, Lyko F, et al. Queuine links translational control in eukaryotes to a micronutrient from bacteria. Nucleic Acids Res. 2019;47: 3711–3727.

16. Hayes P, Fergus C, Ghanim M, Cirzi C, Burtnyak L, McGrenaghan CJ, et al. Queuine Micronutrient Deficiency Promotes Warburg Metabolism and Reversal of the Mitochondrial ATP Synthase in Hela Cells. Nutrients. 2020;12. doi:10.3390/nu12030871

17. Ren D, Mo Y, Yang M, Wang D, Wang Y, Yan Q, et al. Emerging roles of tRNA in cancer. Cancer Lett. 2023;563: 216170.

18. McCarty RM, Somogyi Á, Lin G, Jacobsen NE, Bandarian V. The Deazapurine Biosynthetic Pathway Revealed: In Vitro Enzymatic Synthesis of PreQ0 from Guanosine 5′-Triphosphate in Four Steps. Biochemistry. 2009;48: 3847–3852.

19. Bruender NA, Grell TAJ, Dowling DP, McCarty RM, Drennan CL, Bandarian V. 7-Carboxy-7-deazaguanine Synthase: A Radical S-Adenosyl-l-methionine Enzyme with Polar Tendencies. J Am Chem Soc. 2017;139: 1912–1920.

20. Grell TAJ, Bell BN, Nguyen C, Dowling DP, Bruender NA, Bandarian V, et al. Crystal structure of AdoMet radical enzyme 7-carboxy-7-deazaguanine synthase from Escherichia coli suggests how modifications near [4Fe-4S] cluster engender flavodoxin specificity. Protein Sci. 2019;28: 202–215.

21. Lewis JK, Bruender NA, Bandarian V. QueE: A Radical SAM Enzyme Involved in the Biosynthesis of 7-Deazapurine Containing Natural Products. Methods Enzymol. 2018;606: 95–118.

22. Zhu W, Liu Y. Ring contraction catalyzed by the metal-dependent radical SAM enzyme: 7-carboxy-7-deazaguanine synthase from B. multivorans. Theoretical insights into the reaction mechanism and the influence of metal ions. ACS Catal. 2015;5: 3953–3965.

23. Groisman EA. Feedback Control of Two-Component Regulatory Systems. Annu Rev Microbiol. 2016;70: 103–124.

24. Rao SD, Igoshin OA. Overlaid positive and negative feedback loops shape dynamical properties of PhoPQ two-component system. PLoS Comput Biol. 2021;17: e1008130.

25. Groisman EA. The pleiotropic two-component regulatory system PhoP-PhoQ. J Bacteriol. 2001;183: 1835–1842.

26. Margolin W. FtsZ and the division of prokaryotic cells and organelles. Nat Rev Mol Cell Biol. 2005;6: 862–871.

27. Sun Q, Margolin W. FtsZ dynamics during the division cycle of live Escherichia coli cells. J Bacteriol. 1998;180: 2050–2056.

28. Lippa AM, Goulian M. Feedback inhibition in the PhoQ/PhoP signaling system by a membrane peptide. PLoS Genet. 2009;5: e1000788.

29. Yadavalli SS, Goh T, Carey JN, Malengo G, Vellappan S, Nickels BE, et al. Functional determinants of a small protein controlling a broadly conserved bacterial sensor kinase. J Bacteriol. 2020;202. doi:10.1128/JB.00305-20

30. Horvath DJ Jr, Li B, Casper T, Partida-Sanchez S, Hunstad DA, Hultgren SJ, et al. Morphological plasticity promotes resistance to phagocyte killing of uropathogenic Escherichia coli. Microbes Infect. 2011;13: 426–437.

31. Justice SS, Hunstad DA, Cegelski L, Hultgren SJ. Morphological plasticity as a bacterial survival strategy. Nat Rev Microbiol. 2008;6: 162–168.

32. Jones TH, Vail KM, McMullen LM. Filament formation by foodborne bacteria under sublethal stress. Int J Food Microbiol. 2013;165: 97–110.

33. Abell-King C, Costas A, Duggin IG, Söderström B. Bacterial filamentation during urinary tract infections. PLoS Pathog. 2022;18: e1010950.

34. Dineshkumar TK, Thanedar S, Subbulakshmi C, Varshney U. An unexpected absence of queuosine modification in the tRNAs of an Escherichia coli B strain. Microbiology. 2002;148: 3779–3787.

35. Matuszek Z, Pan T. Quantification of Queuosine Modification Levels in tRNA from Human Cells Using APB Gel and Northern Blot. Bio Protoc. 2019;9: e3191.

36. Christensen DG, Meyer JG, Baumgartner JT, D'Souza AK, Nelson WC, Payne SH, et al. Identification of Novel Protein Lysine Acetyltransferases in Escherichia coli. MBio. 2018;9. doi:10.1128/mBio.01905-18

37. Schilling B, Christensen D, Davis R, Sahu AK, Hu LI, Walker-Peddakotla A, et al. Protein acetylation dynamics in response to carbon overflow in Escherichia coli. Mol Microbiol. 2015;98: 847–863.

38. Kuhn ML, Zemaitaitis B, Hu LI, Sahu A, Sorensen D, Minasov G, et al. Structural, kinetic and proteomic characterization of acetyl phosphate-dependent bacterial protein acetylation. PLoS One. 2014;9: e94816.

39. Vandrisse CM. Escalante-Semerena Protein acetylation in bacteria Annu. Annu Rev Microbiol. 2019;73: 111–132.

40. Fergus C, Barnes D, Alqasem MA, Kelly VP. The queuine micronutrient: charting a course from microbe to man. Nutrients. 2015;7: 2897–2929.

41. Tuorto F, Legrand C, Cirzi C, Federico G, Liebers R, Müller M, et al. Queuosine-modified tRNAs confer nutritional control of protein translation. EMBO J. 2018;37: e99777.

42. McCarty RM, Krebs C, Bandarian V. Spectroscopic, steady-state kinetic, and mechanistic characterization of the radical SAM enzyme QueE, which catalyzes a complex cyclization reaction in the biosynthesis of 7-deazapurines. Biochemistry. 2013;52: 188–198.

43. Madeira F, Pearce M, Tivey ARN, Basutkar P, Lee J, Edbali O, et al. Search and sequence analysis tools services from EMBL-EBI in 2022. Nucleic Acids Res. 2022;50: W276–W279.

44. Jumper J, Evans R, Pritzel A, Green T, Figurnov M, Ronneberger O, et al. Highly accurate protein structure prediction with AlphaFold. Nature. 2021;596: 583–589.

45. Varadi M, Anyango S, Deshpande M, Nair S, Natassia C, Yordanova G, et al. AlphaFold Protein Structure Database: massively expanding the structural coverage of protein-sequence space with high-accuracy models. Nucleic Acids Res. 2022;50: D439–D444.

46. Crooks GE, Hon G, Chandonia J-M, Brenner SE. WebLogo: a sequence logo generator. Genome Res. 2004;14: 1188–1190.

47. Lutkenhaus J. FtsZ ring in bacterial cytokinesis. Mol Microbiol. 1993;9: 403–409.

48. Coltharp C, Xiao J. Beyond force generation: Why is a dynamic ring of FtsZ polymers essential for bacterial cytokinesis? Bioessays. 2017;39: 1–11.

49. Ortiz C, Natale P, Cueto L, Vicente M. The keepers of the ring: regulators of FtsZ assembly. FEMS Microbiol Rev. 2016;40: 57–67.

50. Mingorance J, Rivas G, Vélez M, Gómez-Puertas P, Vicente M. Strong FtsZ is with the force: mechanisms to constrict bacteria. Trends Microbiol. 2010;18: 348–356.

51. Dyer N. Tubulin and its prokaryotic homologue FtsZ: a structural and functional comparison. Sci Prog. 2009;92: 113–137.

52. Mukherjee A, Cao C, Lutkenhaus J. Inhibition of FtsZ polymerization by SulA, an inhibitor of septation in Escherichia coli. Proc Natl Acad Sci U S A. 1998;95: 2885–2890.

53. Justice SS, García-Lara J, Rothfield LI. Cell division inhibitors SulA and MinC/MinD block septum formation at different steps in the assembly of the Escherichia coli division machinery. Mol Microbiol. 2000;37: 410–423.

54. Burby PE, Simmons LA. Regulation of cell division in bacteria by monitoring genome integrity and DNA replication status. J Bacteriol. 2020;202. doi:10.1128/JB.00408-19

55. Wu LJ, Errington J. Coordination of cell division and chromosome segregation by a nucleoid occlusion protein in Bacillus subtilis. Cell. 2004;117: 915–925.

56. Bernhardt TG, de Boer PAJ. SlmA, a nucleoid-associated, FtsZ binding protein required for blocking septal ring assembly over Chromosomes in E. coli. Mol Cell. 2005;18: 555–564.

57. Tonthat NK, Arold ST, Pickering BF, Van Dyke MW, Liang S, Lu Y, et al. Molecular mechanism by which the nucleoid occlusion factor, SlmA, keeps cytokinesis in check. EMBO J. 2011;30: 154–164.

58. Wu LJ, Ishikawa S, Kawai Y, Oshima T, Ogasawara N, Errington J. Noc protein binds to specific DNA sequences to coordinate cell division with chromosome segregation. EMBO J. 2009;28: 1940–1952.

59. Egan AJF, Vollmer W. The physiology of bacterial cell division. Ann N Y Acad Sci. 2013;1277: 8–28.

60. Wang M, Fang C, Ma B, Luo X, Hou Z. Regulation of cytokinesis: FtsZ and its accessory proteins. Curr Genet. 2020;66: 43–49.

61. Harry E, Monahan L, Thompson L. Bacterial cell division: the mechanism and its precison. Int Rev Cytol. 2006;253: 27–94.

62. Miles ZD, McCarty RM, Molnar G, Bandarian V. Discovery of epoxyqueuosine (oQ) reductase reveals parallels between halorespiration and tRNA modification. Proc Natl Acad Sci U S A. 2011;108: 7368–7372.

63. Amann E, Ochs B, Abel KJ. Tightly regulated tac promoter vectors useful for the expression of unfused and fused proteins in Escherichia coli. Gene. 1988;69: 301–315.

64. Goldman SR, Sharp JS, Vvedenskaya IO, Livny J, Dove SL, Nickels BE. NanoRNAs prime transcription initiation in vivo. Mol Cell. 2011;42: 817–825.

65. Hahn J, Maier B, Haijema BJ, Sheetz M, Dubnau D. Transformation proteins and DNA uptake localize to the cell poles in Bacillus subtilis. Cell. 2005;122: 59–71.

66. Briley K Jr, Dorsey-Oresto A, Prepiak P, Dias MJ, Mann JM, Dubnau D. The secretion ATPase ComGA is required for the binding and transport of transforming DNA. Mol Microbiol. 2011;81: 818–830.

67. Schneider CA, Rasband WS, Eliceiri KW. NIH Image to ImageJ: 25 years of image analysis. Nat Methods. 2012;9: 671–675.

68. Ducret A, Quardokus EM, Brun YV. MicrobeJ, a tool for high throughput bacterial cell detection and quantitative analysis. Nat Microbiol. 2016;1: 16077.

69. Rio DC, Ares M Jr, Hannon GJ, Nilsen TW. Purification of RNA using TRIzol (TRI reagent). Cold Spring Harb Protoc. 2010;2010: db.prot5439.

70. Keseler IM, Gama-Castro S, Mackie A, Billington R, Bonavides-Martínez C, Caspi R, et al. The EcoCyc database in 2021. Front Microbiol. 2021;12: 711077.

71. Sievers F, Wilm A, Dineen D, Gibson TJ, Karplus K, Li W, et al. Fast, scalable generation of high-quality protein multiple sequence alignments using Clustal Omega. Mol Syst Biol. 2011;7: 539.

72. Goujon M, McWilliam H, Li W, Valentin F, Squizzato S, Paern J, et al. A new bioinformatics analysis tools framework at EMBL-EBI. Nucleic Acids Res. 2010;38: W695-9.

73. Waterhouse AM, Procter JB, Martin D, Clamp M, Barton GJ. Jalview Version 2 - A multiple sequence alignment editor and analysis workbench. Bioinformatics. 2009;25: 1189–1191.

74. Schneider TD, Stephens RM. Sequence logos: a new way to display consensus sequences. Nucleic Acids Res. 1990;18: 6097–6100.

75. Schrödinger, LLC. The PyMOL Molecular Graphics System, Version 1.8. 2015.

Figure legends

Figure 1. Dual roles of *E. coli* QueE (*Ec*QueE) during stress response. (a) Schematic representation of the dual roles of QueE upon strong activation of the PhoQ/PhoP two-component system. QueE is an enzyme required for the biosynthesis of queuosine (Q) tRNA modification. *E. coli* cells under strong PhoQP-activating stress conditions such as exposure to sub-MIC levels of specific antimicrobial peptides, upregulate QueE, which then modulates cell division in addition to Q biosynthesis. (b) Methods used to study the two activities of QueE – APB (N-acryloyl-3-aminophenylboronic acid) gel and northern blotting to detect Q-tRNAs and microscopy to observe filamentation. (c) APB gel-northern blot detecting $tRNA^{Tyr}$ in total RNA samples of *E. coli* wild-type (WT, MG1655) and Δ*queE* (SAM31) cells encoding either an empty

vector (pEB52) or wild-type (WT) QueE (pRL03). G-tRNA^{Tyr} = unmodified tRNA^{Tyr}, Q-tRNA^{Tyr} = Q-modified tRNA^{Tyr}. (d) Representative phase-contrast micrographs of *E. coli* wild-type (WT, MG1655) and Δ*queE* (SAM31) cells expressing either an empty vector (pEB52) or WT QueE (pRL03), scale bar = 5 µm. For (c) and (d), cells were grown in supplemented MinA minimal medium for 2 hours (OD_{600} = 0.2-0.3) and induced with IPTG ("+") for 3 hours.

Figure 2. Effect of dose-dependent expression of *Ec*QueE on septation. (a) Measurement of cell lengths of *E. coli* MG1655 Δ*lacZYA* (TIM183) cells expressing QueE. Strains containing a plasmid encoding *E. coli* QueE (pRL03) or empty vector (pEB52) were grown in supplemented MinA minimal medium for 2 hours (OD_{600} = 0.2-0.3) and induced with IPTG for 3 hours at the indicated concentration. Gray circles represent individual cells, mean cell length values are indicated in red, and the horizontal gray bars represent the median. Data are obtained from four independent experiments and the number of cells analyzed for each inducer concentration is indicated by (n). Statistical analysis was done using t-test displaying significance at *P ≤ 0.05, **P ≤ 0.01, ***P ≤ 0.001, ****P ≤ 0.0001, and "ns" = P >0.05 (b) Representative phase-contrast micrographs of Δ*lacZYA* cells expressing QueE (pRL03) at the indicated inducer concentration, scale bar = 5 µm.

Figure 3. Effect of single alanine substitutions of conserved amino acid residues in *Ec*QueE on Q biosynthesis and cell division. (a) Structure of *E. coli* QueE (EcQueE, PDB ID 6NHL) showing amino acid residues, catalytically important for Q biosynthesis. (b) Summary of alanine scanning mutagenesis of key amino acid residues in *Ec*QueE and the effect of each mutant on cellular morphology and Q biosynthesis indicated by (+) or (-). (c) APB gel-northern blot detecting tRNA^{Tyr} in total RNA samples of Δ*queE* (SAM31) cells encoding either WT QueE (pRL03), QueE-R27A (pSY98), QueE-C31A (pSA1), QueE-C35A (pSA2) or an empty vector (pEB52). G-tRNA^{Tyr} = unmodified tRNA^{Tyr}, Q-tRNA^{Tyr} = Q-modified tRNA^{Tyr}. (d) Representative

phase-contrast micrographs of Δ*queE* (SAM31) cells expressing WT QueE and selected mutants, scale bar = 5 µm. For (c) and (d), cells were grown in supplemented MinA minimal medium for 2 hours (OD_{600} = 0.2-0.3) and induced with 0.5 mM IPTG for 3 hours.

Figure 4. Role of *Ec*QueE-R27A mutant, deficient in Q biosynthesis, in cell division. (a) Representative phase-contrast and fluorescence micrographs of Δ*queE* (SAM96) cells co-expressing FtsZ-mCherry (pEG4) and either YFP-EcQueE (pSY76) or YFP-*Ec*QueE-R27A (pSA58). Cells were grown in supplemented MinA minimal medium for 4 hours, followed by 0.5% arabinose induction for FtsZ-mCherry expression for another 1 hour (please see Methods for details on pSY76 and derivatives). Green and red arrowheads represent the localization of YFP-QueE and FtsZ- mCherry, respectively. (b) Representative phase-contrast micrographs of Δ*mgrB* and Δ*mgrB*Δ*queE* cells containing either an empty plasmid (pEB52), or plasmids expressing *Ec*QueE (pRL03) and *Ec*QueE-R27A (pSY98), scale bar = 5 µm. Cells were grown in supplemented MinA minimal medium for 2 hours (OD_{600} = 0.2-0.3) and induced with 0.5 mM IPTG for 3 hours. (c) Quantification of YFP-QueE levels in Δ*queE* (SAM96) cells transformed with plasmids encoding YFP-tagged WT *Ec*QueE (pSY76), *Ec*QueE-R27A (pSA58), or an empty vector (pEB52). Cells were grown in supplemented MinA minimal medium for 5 hours. Data represent the mean and range from two independent experiments and fluorescence was quantified from the number of cells (n) per sample as indicated. The red dotted line represents the expression level for WT YFP-QueE. (d) Measurement of cell lengths of Δ*queE* (SAM96) cells encoding WT *Ec*QueE (pRL03), *Ec*QueE-R27A (pSY98), or an empty vector (pEB52). Cells were grown in supplemented MinA minimal medium for 2 hours (OD_{600} = 0.2-0.3) and induced with 0.5 mM IPTG for 3 hours. Gray circles represent individual cells, mean cell length values are indicated in red and the horizontal gray bars represent the median. Data are obtained from three independent experiments and the total number of cells (n) per sample is

indicated. Statistical analysis was done using t-test displaying significance at *P ≤ 0.05, **P ≤ 0.01, ***P ≤ 0.001, ****P ≤ 0.0001, and “ns” = P >0.05.

Figure 5. Analysis of dual functions of QueE among orthologs from *E. coli* and closely related genera. (a) APB gel-northern blot detecting $tRNA^{Tyr}$ in total RNA samples of Δ*queE* (SAM31) cells encoding QueE orthologs from *E. coli* (*Ec*QueE, pRL03), *Bacillus subtilis* (*Bs*QueE, pSY45), *Klebsiella pneumoniae* (*Kp*QueE, pSA5), *Salmonella Typhimurium* St1408 (*St*QueE, pSA21), *Pseudomonas aeruginosa* PA01(*Pa*QueE, pSA127) and an empty vector (pEB52). G-$tRNA^{Tyr}$ = unmodified $tRNA^{Tyr}$, Q-$tRNA^{Tyr}$ = Q-modified $tRNA^{Tyr}$. (b) Representative phase-contrast micrographs of Δ*queE* (SAM31) cells transformed with plasmids encoding either *Ec*QueE, *Bs*QueE, *Kp*QueE, *St*QueE, p*Pa*QueE, or an empty vector, scale bar = 5µm. For (a) and (b), cells were grown in supplemented MinA minimal medium for 2 hours (OD_{600} = 0.2-0.3) and induced with 0.5 mM IPTG for 3 hours. (c) Quantification of YFP-QueE levels in *E. coli* Δ*queE* (SAM96) cells transformed with plasmids encoding YFP-tagged *Ec*QueE (pSY76), *Bs*QueE (pSA121), *Pa*QueE (pSA126), or an empty vector (pEB52). Cells were grown in supplemented MinA minimal medium for 5 hours (please see Methods for details on pSY76 and derivatives). Data represent the mean and range from two independent experiments, and fluorescence was quantified from the number of cells (n) per sample as indicated. The red dotted line represents the expression level for WT YFP-QueE, Statistical analysis was done using t-test displaying significance at *P ≤ 0.05, **P ≤ 0.01, ***P ≤ 0.001, ****P ≤ 0.0001, and “ns” = P >0.05.

Figure 6. Role of region E45-W67 in *E. coli* QueE in the biosynthesis of Q-tRNA modification. (a) Structural alignment of *E. coli* QueE (*Ec*QueE, PDB 6NHL, dark gray), *Bacillus subtilis* QueE (*Bs*QueE, PDB 5TH5, light gray), and an Alphafold-generated model of *P. aeruginosa* QueE (*Pa*QueE, cyan). The variable region E45-W67 in *Ec*QueE is highlighted in

red. (b) APB gel-northern blot showing Q-tRNA profiles of Δ*queE* cells (SAM31) containing IPTG inducible plasmids encoding *E. coli* QueE (pRL03), control vector (pEB52), and selected mutants of *Ec*QueE - pQueE-ΔE45-E51 (pSA60), pQueE-ΔV52-W67 (pSA61), and pQueE-ΔE45-W67 (pSA62). G-tRNA^{Tyr} = unmodified tRNA^{Tyr}, Q-tRNA^{Tyr} = Q-modified tRNA^{Tyr} (c) Phase contrast micrographs of Δ*queE* (SAM31) cells transformed with an empty vector and plasmids encoding Wildtype (WT) *Ec*QueE and the selected *Ec*QueE peptide deletion mutants (as in (a) above), Scale bar = 5 µm. For (b) and (c), cells were grown in supplemented MinA minimal medium for 2 hours (OD_{600} = 0.2-0.3) and induced with 0.5 mM IPTG for 3 hours. (d) Quantification of QueE levels in Δ*queE* (SAM96) cells transformed with an empty vector and IPTG inducible plasmids encoding YFP-tagged wild-type QueE (WT, pSY76) and QueE ΔE45-W67 (pSA76). Cells were grown in supplemented MinA minimal medium for 5 hours (please see Methods for details on pSY76 and derivatives). Dots and the error bars represent the mean and range from two independent experiments with quantified fluorescence, and the total number of cells (n) per sample is indicated. The red dotted line represents the expression levels for WT. Statistical analysis was done using t-test displaying significance at *P ≤ 0.05, **P ≤ 0.01, ***P ≤ 0.001, ****P ≤ 0.0001, and “ns” = P >0.05.

Figure 7. QueE’s dual roles in Q-biosynthesis and septation inhibition. (a) Structure of *E. coli* QueE (PDB 6NHL) showing residue affecting Q-biosynthesis only (green, R27) and septation inhibition only (red, C31, C35, E45-W67). (b) A consensus sequence of the E45-W67 region from 18 representative enterobacteria (see Fig S8 for details) was generated using WebLogo [46].

Supporting Information

Tables

Table A. List of strains used in the study

Strain	Relevant genotype	Reference/source
MG1655	*λ⁻ rph⁻¹*	*E. coli* Genetic Stock Center, CGSC no. 7740
SAM31	MG1655 *ΔqueE* λ_{att} (P_{mgrB}-*yfp*) HK_{att} (P_{tetA}-*cfp*)	Goulian lab
SAM54	MG1655 *ΔqueE* MG1655 Φ(*queE*⁺ -*yfp*⁺) KanR	[1]
SAM96	MG1655 *ΔqueE*	[1]
TIM183	MG1655 Δ*lacZYA*	
Top10	*F– mcrA Δ(mrr-hsdRMS-mcrBC) φ80lacZΔM15 ΔlacX74 recA1 araD139 Δ(ara-leu)7697 galU galK λ– rpsL (StrR) endA1 nupG*	Invitrogen
XL1-Blue	*recA1 endA1 gyrA96 thi-1 hsdR17 supE44 relA1 lac [F´ proAB lacIqZΔM15 Tn10 (Tetr)]*	[2]
S. Typhimurium 14208	*Salmonella enterica subsp. enterica* (ex-Kauffmann and Edwards) Le Minor and Popoff serovar Typhimurium, ATCC 14028	Schifferli lab
Klebsiella pneumoniae 13883	*Klebsiella pneumoniae subsp. pneumoniae* (Schroeter) Trevisan 13883	Fan lab
P. aeruginosa PAO1	*lacI*$^{q+}$ *Δ*(*lacZ*)M15⁺ *tetA*⁺ *tetR*⁺	Nickels lab
B. subtilis 168	*trpC2*	Boyd lab
B. subtilis IS75	His⁻ Leu⁻ Met⁻, *amyE*⁺	Dubnau lab
SAA50	*B. subtilis* IS75 Δ*amyE*::pSA147 (*BsqueE*)	This work
SAA52	*B. subtilis* IS75 Δ*amyE*::pSA149 (*yfp-BsqueE*)	This work
SAA53	*B. subtilis* IS75 Δ*amyE*::pPDR111 (*empty*)	This work

Table B. List of plasmids used in the study

Name	Description	Reference/source
pBAD33	ori(p15A), ParaBAD-MCS araC, camR	ATCC 87402
pDR111	amyE-hyper-SPANK, specR, carbR.	Dubnau lab

pEB52	pTrc99a with the NcoI site removed, carbR	Goulian lab
pEG4	pBAD33 ftsZ-mCherry, camR	[3]
pPSV38	Shuttle vector, *lacI*^{q}, *lacUV5* promoter, origins of replication, *colE1* and pRO1600*,* gentR	Dove lab
pRL03	pEB52-EcQueE carbR	[1]
pSA1	pEB52-EcQueE C31A, carbR	This work
pSA2	pEB52-EcQueE C35A, carbR	This work
pSA3	pEB52-EcQueE C38A, carbR	This work
pSA5	pEB52-EcQueE E15A, carbR	This work
pSA8	pEB52-EcQueE S136A, carbR	This work
pSA9	pEB52-EcQueE K60A, carbR	This work
pSA10	pEB52-EcQueE K66A, carbR	This work
pSA11	pEB52-EcQueE K194A, carbR	This work
pSA21	pEB52-StQueE, carbR	This work
pSA22	pEB52-PaQueE, carbR	This work
pSA55	pEB52-EcQueE W67A, carbR	This work
pSA57	pEB52-yfp-EcQueE K66A, carbR	This work
pSA58	pEB52-yfp-EcQueE R27A, carbR	This work
pSA59	pBAD33-KpQueE, camR	This work
pSA60	pRL03-QueE ΔE45-E51, carbR	This work
pSA61	pRL03-QueE ΔV52-W67, carbR	This work
pSA62	pRL03-QueE ΔE45-W67, carbR	This work
pSA73	pEB52-yfp-EcQueE E15A, carbR	This work
pSA75	pEB52-yfp -EcQueE C31A, carbR	This work
pSA76	pEB52-yfp-EcQueE ΔE45-W67	This work
pSA119	pEB52-yfp-QueE C35A, carbR	This work
pSA121	pEB52-yfp-pBsQueE, carbR	This work

pSA126	pEB52-yfp-pPaQueE, carbR	This work
pSA147	pDR111-BsQueE, specR, carbR.	This work
pSA149	pDR111-yfp-BsQueE, specR, carbR.	This work
pSA151	pUCP20T-PaQueE, carbR	This work
pSA154	pPSV38-yfp-PaQueE, gentR	This work
pSA156	pPSV38-PaQueE, gentR	This work
pSA157	pPSV38-EcQueE, gentR	This work
pSY45	pEB52-BsQueE, carbR	This work
pSY76	pEB52-yfp-QueE, contains a strong ribosome binding site (AAAGAGGAGA), no IPTG induction required, carbR	[1]
pSY85	pEB52-His_6-QueE, carbR	This work
pSY97	pEB52-EcQueE Q13A, carbR	This work
pSY98	pEB52-EcQueE R27A, carbR	This work
pSY99	pEB52-EcQueE T40A, carbR	This work
pSY100	pEB52-EcQueE Q189A, carbR	This work
pTrc99a	Expression vector, pBR322 ori, pTrc promoter, *lacI*^{q}, carbR	[4]
pUCP20 T-eyfp	Shuttle vector encoding YFP, *lacUV5* promoter, origins of replication, *colE1* and pRO1600, carbR	Addgene #78466

carbR = carries a carbenicillin/ampicillin-resistance marker; camR = carries a chloramphenicol-resistance marker

Table C. List of oligonucleotides used in the study

Name of Primer	5' - 3'	Reference/source
SA1	TACAGTCTGCTCCCTTTGGCCGCTCGGGAAC CCCAC	Probe for tyrU gene
SA3F	GCCCCGGTTGGCTGTGCCTG	Inv PCR Primer for C31A
SA3R	TCCCTGTAAACGAATAAAAATGGCGG	Inv PCR Primer for C31A
SA4F	GCCGCCTGGTGCGACACCAAACAC	Inv PCR Primer for C35A

SA4R	GCCAACCGGGCATCCCTGTAAACG	Inv PCR Primer for C35A
SA7F	ACCTTGCAGGGTCTGGAACATCTCG	Inv PCR Primer for E15A
SA7R	GCCGGTTACTTTACCGGCGTTCCCG	Inv PCR Primer for E15A
SA9F	GCCGAGCCTTGCATTCATGATTTGCTGCC	Inv PCR Primer for G94A
SA9R	ACCCGTAATCACCACATGCCGC	Inv PCR Primer for G94A
SA11F	GTTGGCTGTGCCTGGGCCGACACCAAACACAC	Single Primer SDM for C38A in *E. coli* QueE
SA13F	GCCTGGGGGGCTGCGAGCAGTG	Inv PCR Primer for K66A
SA13R	ATCACTCTCTTTGGTCTTCGCCAG	Inv PCR Primer for K66A
SA12F	GCCACCAAAGAGAGTGATAAGTGGG	Inv PCR Primer for K60A
SA12R	CGCCAGAATGCTGAAAAGGGA	Inv PCR Primer for K60A
SA10F	GCCCCAAAGCTGAACATGCGCGGC	Inv PCR Primer for S136
SA10R	TACGGTAACCCAGGTATTCGGTGTGC	Inv PCR Primer for S136
SA5F	GCCGACACCAAACACACCTGGG	Inv PCR Primer for C38A
SA5R	CAGGCACAGCCAACCGGGC	Inv PCR Primer for C38A
queE-Q189A-L1	CAGTGCAATGACTCGCGGTTTATCATC	Inv PCR Primer for Q189A
queE-Q189A-U1	gcgCCGATTAGCCAAAAGGATGATGCCA	Inv PCR Primer for Q189A
queE-T40A-L1	GTCGCACCAGGCACAGCCAAC	Inv PCR Primer for T40A
queE-T40A-U1	gcgAAACACACCTGGGAAAAGCTTGAG	Inv PCR Primer for T40A
queE-R27A-L1	AATAAAAATGGCGGGAACGCCG	Inv PCR Primer for R27A
queE-R27A-U1	gcgTTACAGGGATGCCCGGTTGG	Inv PCR Primer for R27A
queE-Q13A-L1	CAGGGTCTGGAACATCTCGTTAATCG	Inv PCR Primer for Q13A
queE-Q13A-U1	gcgGGTGAGGGTTACTTTACCGGC	Inv PCR Primer for Q13A
SA79F	GCGTTACAGGGATGCCCGGTTGG	R27A F-primer
SA79R	AATAAAAATGGCGGGAACGCCG	R27A R-primer
SA80F	aaattaagcATGCAGTACCCGATTAACGAGATG	Adds RBS to pSA56
SA80R	ctcctctttaatGgtaccgagctcgaattcg	Adds RBS to pSA56
SA26R	CATCCGCCAAAACAGCCAAG	Seq R-Primer for pEB52 inserts
Bs_queE-SacI-U1	GACTACGAGCTCAAAAGGGTGGTTTGAATGGCTAAAG	BsQueE in pEB52
Bs_queE-BamHI-L1	AGTAGTGGATCCCTATTATACTCCGCGTTTGTTGCC	BsQueE in pEB52
SA28F	CAGAGAATTCatgGTTTCAGCTCGGCTGATCTTC	StQueE in pEB52
SA28R	TAGAGGATCCtcaATGGCCCGGTTCGTCG	StQueE in pEB52
SA29F	CAGAGAATTCATGCAGTACCCGATTAACGAAATGTTCC	PaQueE
SA29R	TAGAGGATCCTCAGGCGATATTTAAATACTTATGCGTTTGC	PaQueE

SA78F	ATTAGGTACCATGCAGTACCCGATTAACGAGATGTTC	KpQueE in pBAD33
SA78R	ATTATCTAGATCAGGCAATATTCAGATACTTGTGCGTC	KpQueE in pBAD33
SA81F	ggcagcggcGTCTCCCTTTTCAGCATTCTGGCG	Inverse PCR Primer to remove E45-E51 to pRL03
SA81R	gctgccgccCCAGGTGTGTTTGGTGTCG	Inverse PCR Primer to remove E45-E51 to pRL03
SA82F	ggcagcggcGGGGCTGCGAGCAGTGAAG	Inverse PCR Primer to remove V52-W67 to pRL03
SA82R	gctgccgccTTCCCGATCCTCAAGCTTTTCCC	Inverse PCR Primer to remove V52-W67 to pRL03
SA69F	Ccataagattagcggatcctacctgac	pBAD33 Forward sequencing primer
SA69R	tcagaccgcttctgcgttc	pBAD33 Reverse sequencing primer
SA125R_pSY76_R	tctagtTTTGTATAGTTCATCCATGCCATGTG	Hifi assembly vector primer
SA125F_pSY76_Bs	CAACAAACGCGGAGTAtaaTTAAACATTTATAAGCGTTATAAATGGGTGGAACC	Hifi assembly vector primer for BsQueE
SA125F_pSY76_Pa	GAACCGGGCCATtgaTTAAACATTTATAAGCGTTATAAATGGGTGGAACC	Hifi assembly vector primer for PaQueE
SA126F_Bs_F	CATGGATGAACTATACAAAactagaatgGCTAAAGGAATTCCTGTATTAGAAATTTTCGG	Hifi assembly insert primer for BsQueE
SA126R_Bs_R	ttaTACTCCGCGTTTGTTGCCC	Hifi assembly insert primer for BsQueE
SA127F_Pa_R	TTAAtcaATGGCCCGGTTCGTC	Hifi assembly insert primer for PaQueE
SA127R_Pa_Corr_F	CATGGATGAACTATACAAAactagaatgCAACAGACCCTGCGC	Hifi assembly insert primer for PaQueE
SA149_BsQueE_F	TATATGTCGACTGAAAGGAGAGGGAATCAAATTGGCTAAAGGAATTCCTGTATTAGAAATTTTCG	Cloning BsQueE with a Sal1 cut site.
SA149_BsQueE_R	TATATGCTAGCTTATACTCCGCGTTTGTTGCCC	Cloning BsQueE with a Nhe1 cut site
SA150_YFP_BsQueE_F SA1	TATATGTCGACTGAAAGGAGAGGGAATCAAATTGCGTAAAGGAGAAGAACTTTTCACTGG	Cloning YFP-BsQueE with a Sal1 cut site
SA157R	CTGGCGAAAGGGGGATGTG	Forward Sequencing primer for pUCP20T vector and its derivatives
SA157F	CACTTTATGCTTCCGGCTCGTATG	Reverse Sequencing primer for pUCP20T vector and its derivatives
SA155F	CTAGAATTAAAGAGGAGAAATTAAGCATGCAACAGACCCTGCGC	Forward primer to clone PaQueE into pUCP20T
SA154R	CCAAGAAGGTCTAGAATTAAAGAGGAGAAATTAAGCATGCGTAAAGG	Reverse primer to clone PaQueE into pUCP20T

SA157R	CTGGCGAAAGGGGGATGTG	Forward Sequencing primer for pSA151
SA157F	CACTTTATGCTTCCGGCTCGTATG	Reverse Sequencing primer for pSA151
SA25F	TCGTATAATGTGTGGAATTGTGAGCG	Forward Sequencing primer for pSA126

Figures

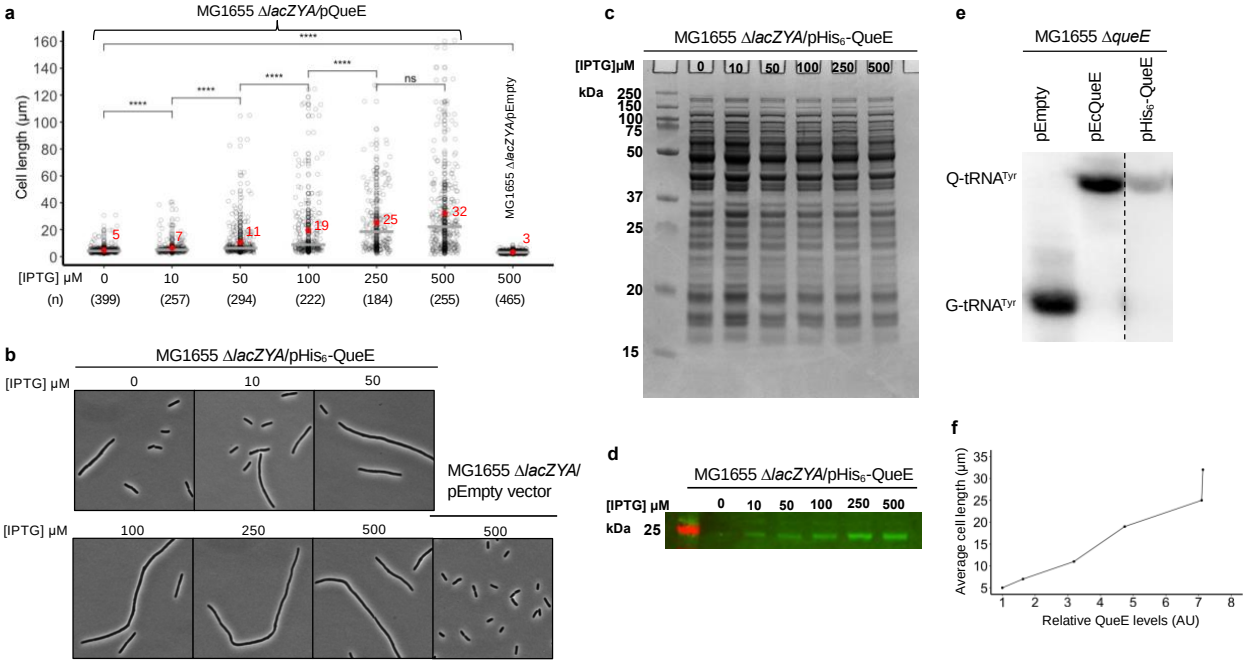

Figure S1. His_6-tagged QueE regulates septation in a dose-dependent manner. (a) Measurement of cell lengths of *E. coli* MG1655 Δ*lacZYA* (TIM183) cells expressing QueE. Strains containing a plasmid encoding *E. coli* His_6-*Ec*QueE (pSY85) or empty vector (pEB52) were grown in supplemented MinA minimal medium for 2 hours (OD_{600} = 0.2-0.3) and induced with IPTG for 3 hours at the indicated concentration. Gray circles represent individual cells, mean cell length values are indicated in red, and the horizontal gray bars represent the median. Data are obtained from four independent experiments using the number of cells indicated by (n) for each inducer concentration. Statistical analysis was done using t-test displaying significance at *P ≤ 0.05, **P ≤ 0.01, ***P ≤ 0.001, ****P ≤ 0.0001, and "ns" = P >0.05 (b) Representative phase-contrast micrographs of Δ*lacZYA* cells expressing QueE at the indicated inducer concentration, scale bar = 5 µm. (c-d) Representative Coomassie gel showing protein levels in total cell lysates at different IPTG concentrations and the corresponding western blot showing His_6-QueE levels. e) APB gel-northern blot detecting $tRNA^{Tyr}$ in total RNA samples of Δ*queE* (SAM31) cells encoding either WT QueE (pRL03), His_6-QueE (pSY85) or an empty vector (pEB52). Cells were grown in supplemented MinA minimal medium for 2 hours and induced with 0.5 mM IPTG for 3 hours. G-$tRNA^{Tyr}$ = unmodified $tRNA^{Tyr}$, Q-$tRNA^{Tyr}$ = Q-modified $tRNA^{Tyr}$. Note that this panel is a montage with the data for $pHis_6$-QueE acquired on another blot, as indicated with a dotted line. (f) Plot showing the relationship between average cell lengths (from panel a) and relative QueE abundance (from panel d), see methods for details.

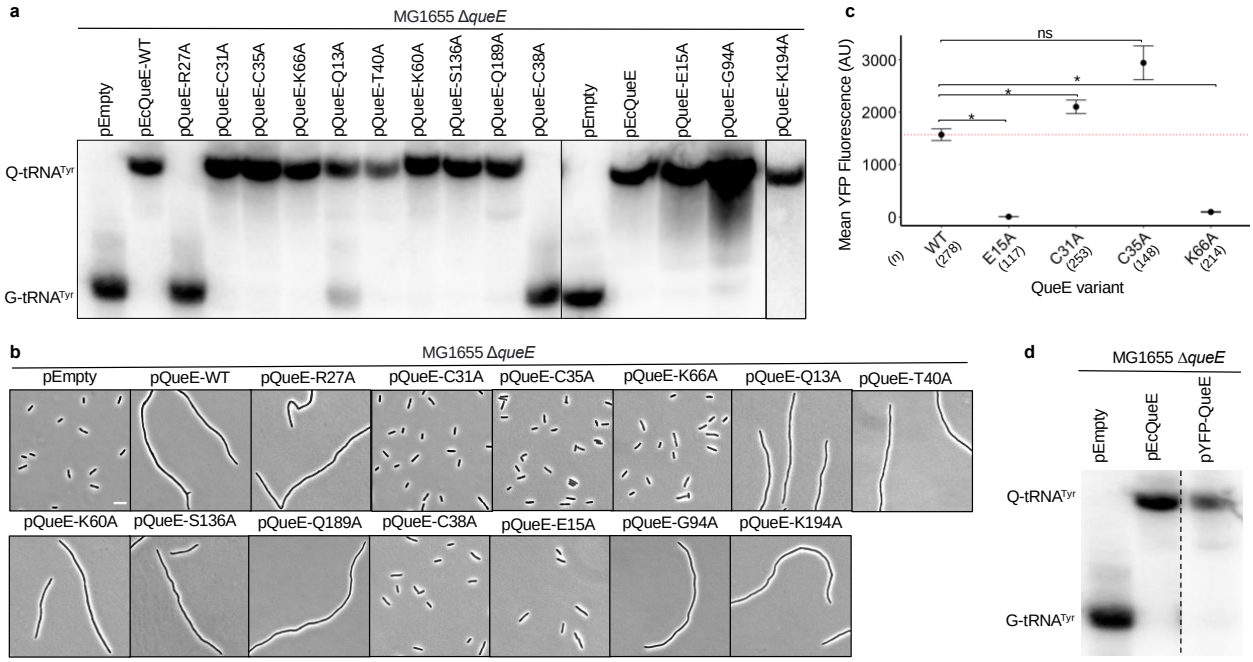

Figure S2. Alanine scanning mutagenesis of amino acid residues in *Ec*QueE important for Q biosynthesis. (a) APB northern blot detecting $tRNA^{Tyr}$ in total RNA samples of Δ*queE* (SAM31) cells encoding either WT QueE (pRL03), QueE variants, QueE-R27A (pSY98), QueE-C31A (pSA1), QueE-C35A (pSA2.6), QueE-K66A (pSA10), QueE-Q13A (pSY97), QueE-T40A (pSY99), QueE-K60A (pSA9), QueE-S136A (pSA8), QueE-Q189A (pSY100), QueE-C38A (pSA3) or an empty vector (pEB52). Cells were grown in supplemented MinA minimal medium for 2 hours and induced with 0.5 mM IPTG for 3 hours. G-$tRNA^{Tyr}$ = unmodified $tRNA^{Tyr}$, Q-$tRNA^{Tyr}$ = Q-modified $tRNA^{Tyr}$. (b) Representative phase-contrast micrographs of Δ*queE* (SAM31) cells expressing WT QueE and single alanine mutants as indicated above in (a), scale bar = 5 µm. Cells were grown in supplemented MinA minimal medium for 2 hours and induced with 0.5 mM IPTG for 3 hours. (c) Quantification of levels of YFP-tagged QueE and its variants in Δ*queE* (SAM96) cells transformed with plasmids encoding WT YFP-QueE (pSY76), YFP-QueE-E15A (pSA73), YFP-QueE-C31A (pSA75), YFP-QueE-C35A (pSA119), or YFP-QueE-K66A (pSA57). Cells were grown in supplemented MinA minimal medium for 5 hours. Data represent the mean and range from two independent experiments, and fluorescence was quantified from the number of cells (n) per sample as indicated. The red dotted line represents the expression level for WT YFP-QueE, Statistical analysis was done using t-test displaying significance at *P ≤ 0.05, **P ≤ 0.01, ***P ≤ 0.001, ****P ≤ 0.0001, and “ns” = P >0.05. (d) APB gel- northern blot detecting $tRNA^{Tyr}$ in total RNA samples of Δ*queE* (SAM31) cells encoding either WT QueE (pRL03), YFP-QueE (pSY76) or an empty vector (pEB52). Cells were grown in supplemented MinA minimal medium for 2 hours and induced with 0.5 mM IPTG for 3 hours. Cells expressing YFP-QueE were grown in supplemented MinA minimal medium for 5 hours (please see Methods for details on pSY76). G-$tRNA^{Tyr}$ = unmodified $tRNA^{Tyr}$, Q-$tRNA^{Tyr}$ = Q-

modified $tRNA^{Tyr}$. Note that this panel is a montage with the data for pYFP-QueE acquired on another blot, as indicated with a dotted line.

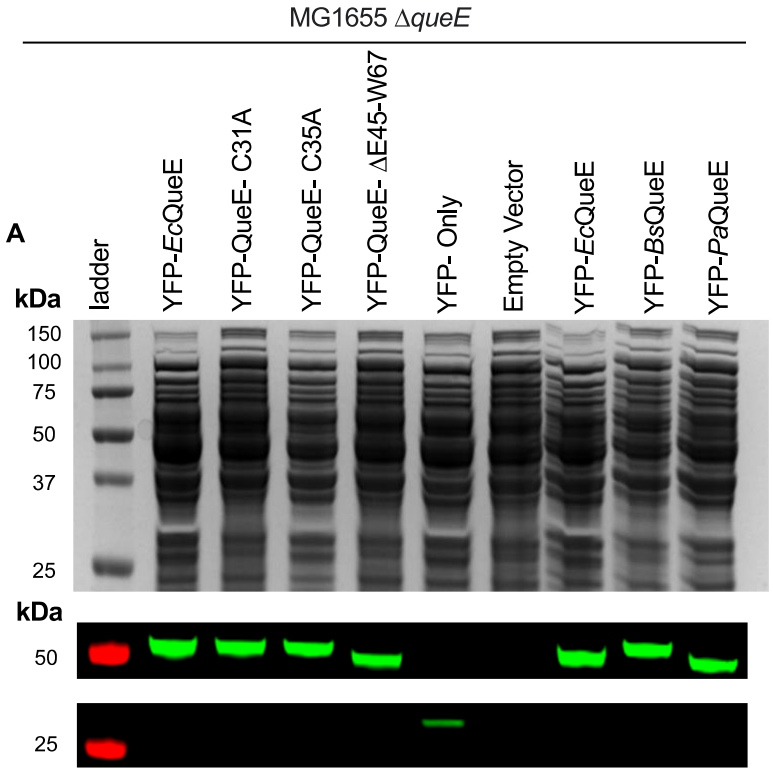

Figure S3. Analysis of YFP-tagged variants of *E. coli* QueE and orthologs. (a) Coomassie stain and (b) western blots of cell lysates of *E. coli* strains encoding YFP-tagged *Ec*QueE (pSY76), its variants C31A (pSA75), C35A (pSA119), ΔE45-W67 (pSA76), and QueE orthologs *Bs*QueE (pSA121) and *Pa*QueE (pSA126). Lysates were prepared from cells grown in supplemented MinA minimal medium for 5 hours (please see Methods for details on pSY76 and derivatives). Cells from a strain carrying a genomic *yfp* reporter (SAM54) are indicated as YFP-only control.

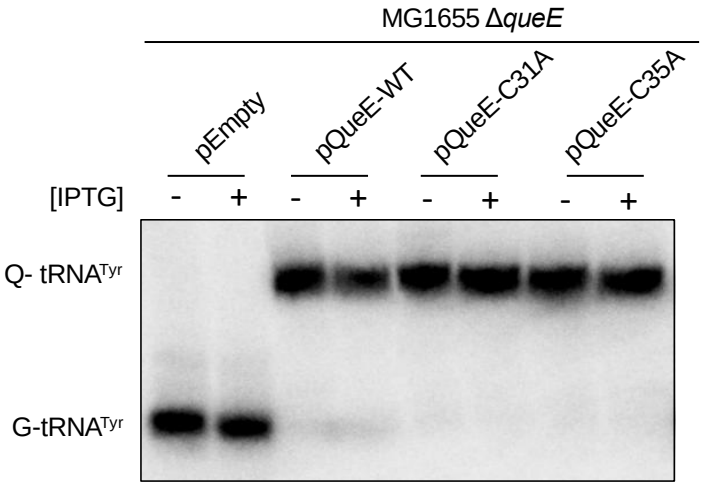

Figure S4. Q-tRNA formation in cells expressing QueE variants (QueE-C31A and -C35A). APB gel-northern blot detecting tRNA^{Tyr} in total RNA samples of Δ*queE* (SAM31) cells carrying either an empty vector (pEB52), WT QueE (pRL03), QueE-C31A (pSA1) or QueE-C35A (pSA2). G-tRNA^{Tyr} = unmodified tRNA^{Tyr}, Q-tRNA^{Tyr} = Q-modified tRNA^{Tyr}. Cells were grown in supplemented MinA minimal medium for 2 hours and induced with 0.5 mM IPTG as indicated (+).

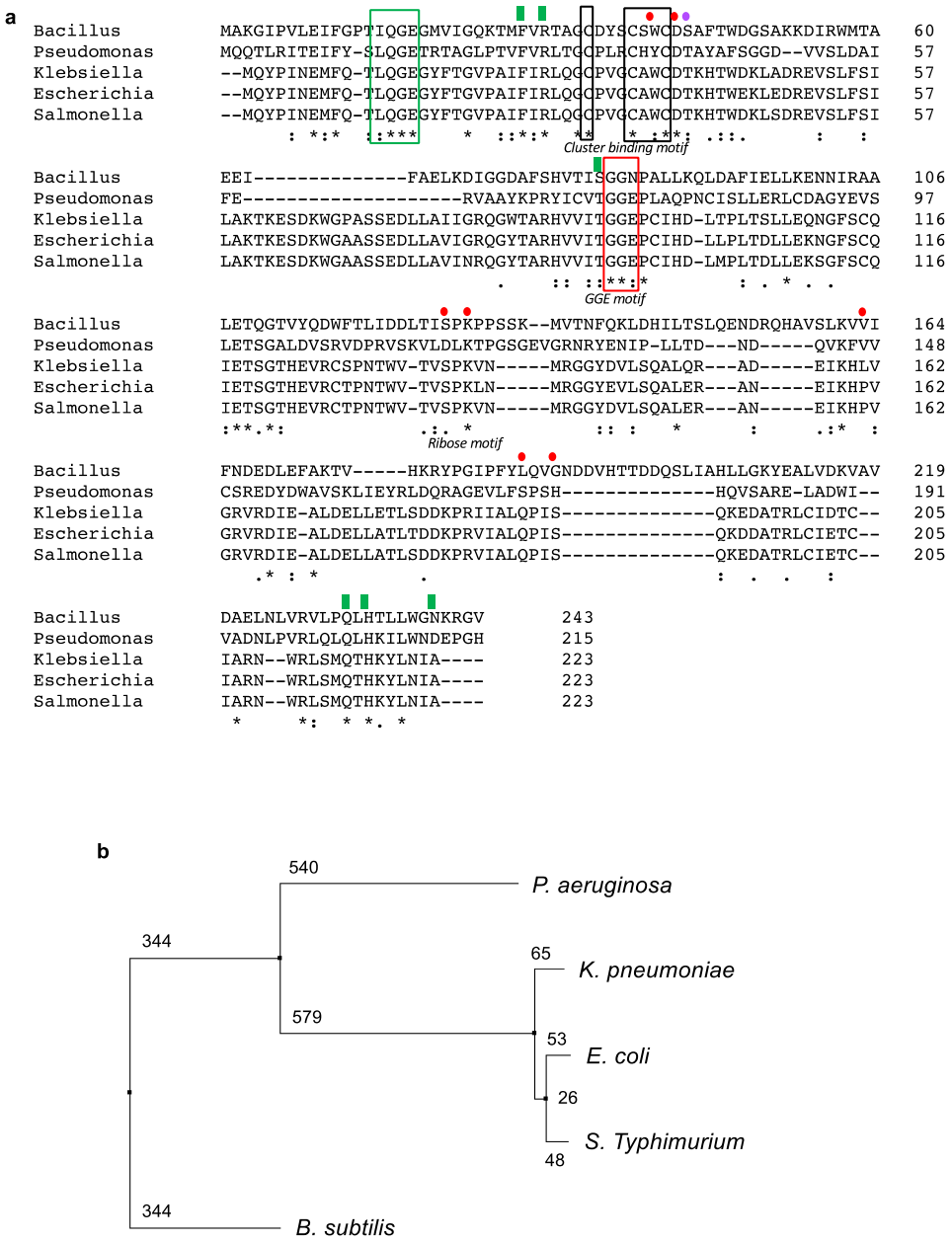

Figure S5. Sequence analysis and phylogeny of selected QueE orthologs. (a) Multiple sequence alignment of QueE orthologs from *Bacillus subtilis* str 168, *Pseudomonas aeruginosa* PA01, *Klebsiella pneumoniae*, *Escherichia coli K-12 MG1655*, and *Salmonella Typhimurium* St1408. The cluster binding motif residues are boxed in black, and residues involved in binding S-adenosyl methionine are highlighted using red circles (single residues) and red boxes (sequential residues). Residues involved in substrate binding (CPH_4/6-CP ligation) are denoted by green rectangles (single residues) and green boxes (sequential residues). A single amino acid residue involved in binding the catalytic magnesium ion is indicated by a purple circle. (b) Phylogenetic tree of the QueE orthologs estimated by the neighbor-joining method (BLOSUM62) using Jalview[5].

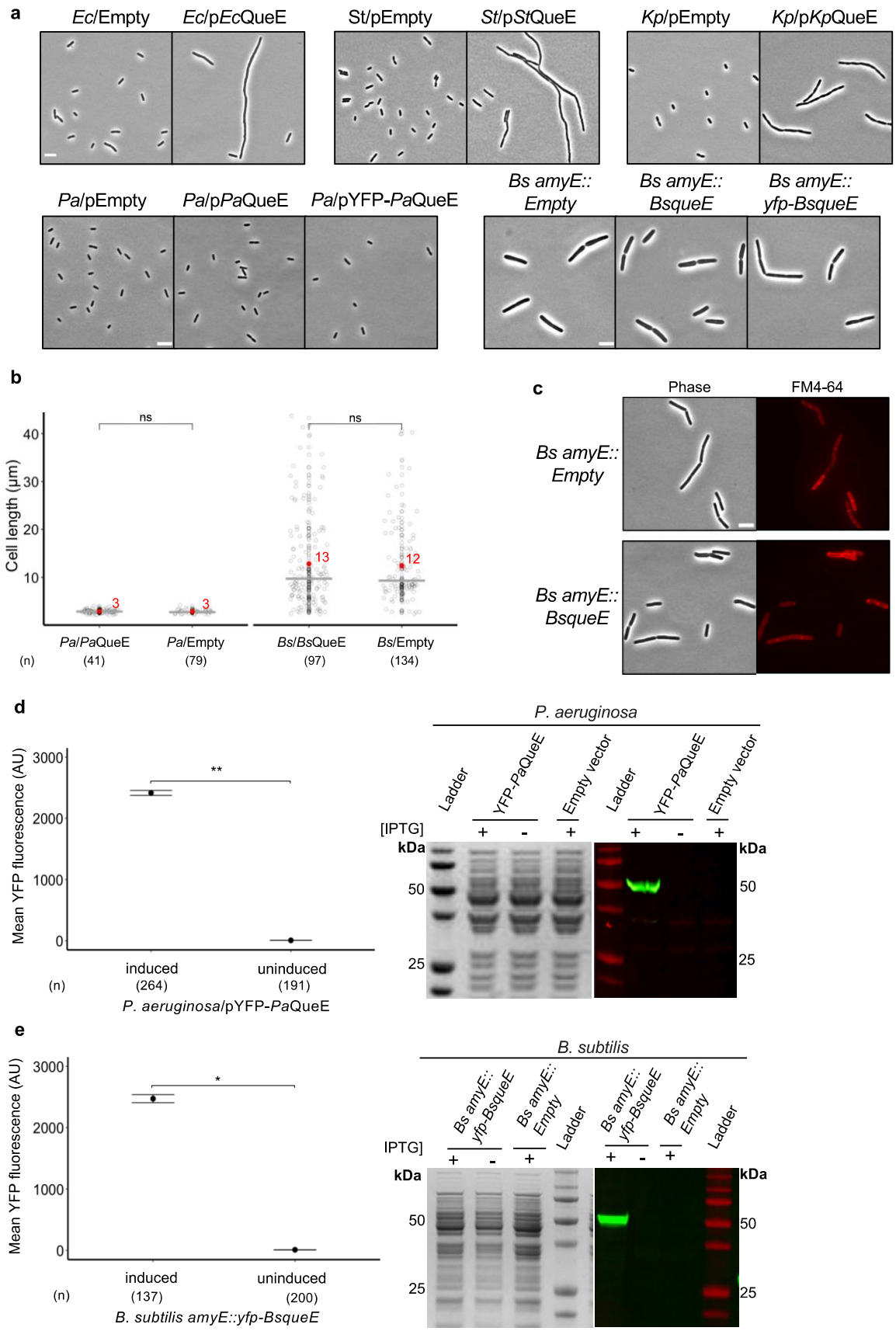
a
Ec/Empty
Ec/pEcQueE
St/pEmpty
St/pStQueE
Kp/pEmpty
Kp/pKpQueE
Pa/pEmpty
Pa/pPaQueE
Pa/pYFP-PaQueE
Bs amyE:: Empty
Bs amyE:: BsqueE
Bs amyE:: yfp-BsqueE
b
Cell length (µm)
ns
ns
3
3
13
12
Pa/PaQueE
Pa/Empty
Bs/BsQueE
Bs/Empty
(n)
(41)
(79)
(97)
(134)
c
Phase
FM4-64
Bs amyE:: Empty
Bs amyE:: BsqueE
d
Mean YFP fluorescence (AU)
**
induced
uninduced
(n)
(264)
(191)
P. aeruginosa/pYFP-PaQueE
P. aeruginosa
Ladder
YFP-PaQueE
Empty vector
[IPTG]
kDa
50
25
e
Mean YFP fluorescence (AU)
*
induced
uninduced
(n)
(137)
(200)
B. subtilis amyE::yfp-BsqueE
B. subtilis
Bs amyE:: yfp-BsqueE
Bs amyE:: Empty
Ladder
IPTG]
kDa
50
25

Figure S6. Analysis of dual functions of *Ec*QueE orthologs in their hosts. (a) Representative phase-contrast micrographs of *E. coli, Salmonella Typhimurium*, *Klebsiella pneumoniae*, *Pseudomonas aeruginosa*, and *Bacillus subtilis* expressing their native QueE ortholog. The corresponding plasmid constructs are indicated, p*Ec*QueE (pRL03), p*St*QueE (pSA21), p*Kp*QueE (pSA59), p*Pa*QueE (pSA156), pYFP-*Pa*QueE (pSA154). Empty vectors pEB52 for *E. coli*, *S. Typhimurium*, pBAD33 for *K. pnueumoniae*, pPSV38 for *P. aeruginosa*) were included as controls. *B. subtilis* strains encoding *Bs*QueE (*Bs amyE::Bs*QueE, SAA50) and YFP-*Bs*QueE (*Bs amyE::yfp-Bs*QueE, SAA52) at the genomic *amyE* locus are indicated and *B. subtilis* strain carrying empty vector pDR111 sequence at *amyE* locus (*Bs amyE::Empty*, SAA53) was included as a control. All cultures were grown in supplemented MinA minimal medium and QueE expression was induced using 0.5 mM IPTG in all cases, except for *P. aeruginosa* and *B. subtilis* where IPTG was used at 2 mM and 1 mM, respectively. Scale bar = 5µm. (b) Measurement of cell lengths of *B. subtilis* expressing *Bs*QueE (*Bs amyE::Bs*QueE, SAA50), control strain (*Bs amyE::Empty*, SAA53), *P. aeruginosa* cells expressing *Pa*QueE (pSA156), or an empty vector (pPSV38). QueE expression was induced using IPTG at 2 mM and 0.5 mM for *P. aeruginosa* and *B. subtilis*, respectively. Gray circles represent individual cells, mean cell length values are indicated in red, and the horizontal gray bars represent the median. Data are obtained from two independent experiments using (n) number of cells per sample as indicated for each strain, Statistical analysis was done using t-test displaying significance at *P ≤ 0.05, **P ≤ 0.01, ***P ≤ 0.001, ****P ≤ 0.0001, and “ns” = P >0.05. (c) FM 4-64 staining of *B. subtilis* cells expressing either *Bs*QueE (*Bs amyE::Bs*QueE, SAA50) or control strain (*Bs amyE::Empty*, SAA53), QueE expression was induced using 0.5 mM IPTG. Scale bar = 5µm. (d) Quantification of levels of YFP-tagged *Pa*QueE (pSA154) expressed in *P. aeruginosa* with or without induction with 2 mM IPTG, normalized to the background fluorescence in cells carrying an empty vector (pPSV38). Data are obtained from two independent experiments using (n) number of cells per sample as indicated. The corresponding Coomassie-stained gel and western blots show *Pa*QueE protein expression in total cell lysates. (e) Quantification of levels of YFP-tagged *Bs*QueE expressed in *B. subtilis* (Bs *amyE::yfp-Bs*QueE, SAA52) with or without induction with 0.5 mM IPTG, normalized to the background fluorescence in control (*Bs amyE::Empty*, SAA53). Data are obtained from two independent experiments using (n) number of cells per sample as indicated. The corresponding Coomassie-stained gel and western blots show *Bs*QueE protein expression in total cell lysates.

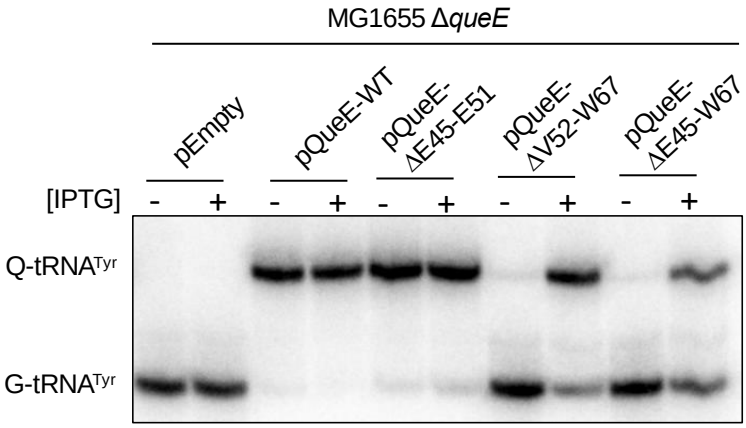

Figure S7. Q-tRNA formation in cells expressing QueE deletion mutants (QueE-ΔE45-E51, -ΔV52-W67, and -ΔE45-W67). APB gel-northern blot detecting tRNA^{Tyr} in total RNA samples of Δ*queE* (SAM31) cells carrying either an empty vector (pEB52), WT QueE (pRL03), QueE-ΔE45-E51 (pSA60), QueE-ΔV52-W67 (pSA61), or QueE-ΔE45-W67 (pSA62). G-tRNA^{Tyr} = unmodified tRNA^{Tyr}, Q-tRNA^{Tyr} = Q-modified tRNA^{Tyr}. Cells were grown in supplemented MinA minimal medium for 2 hours and induced with 0.5 mM IPTG as indicated (+) for 3 hours.

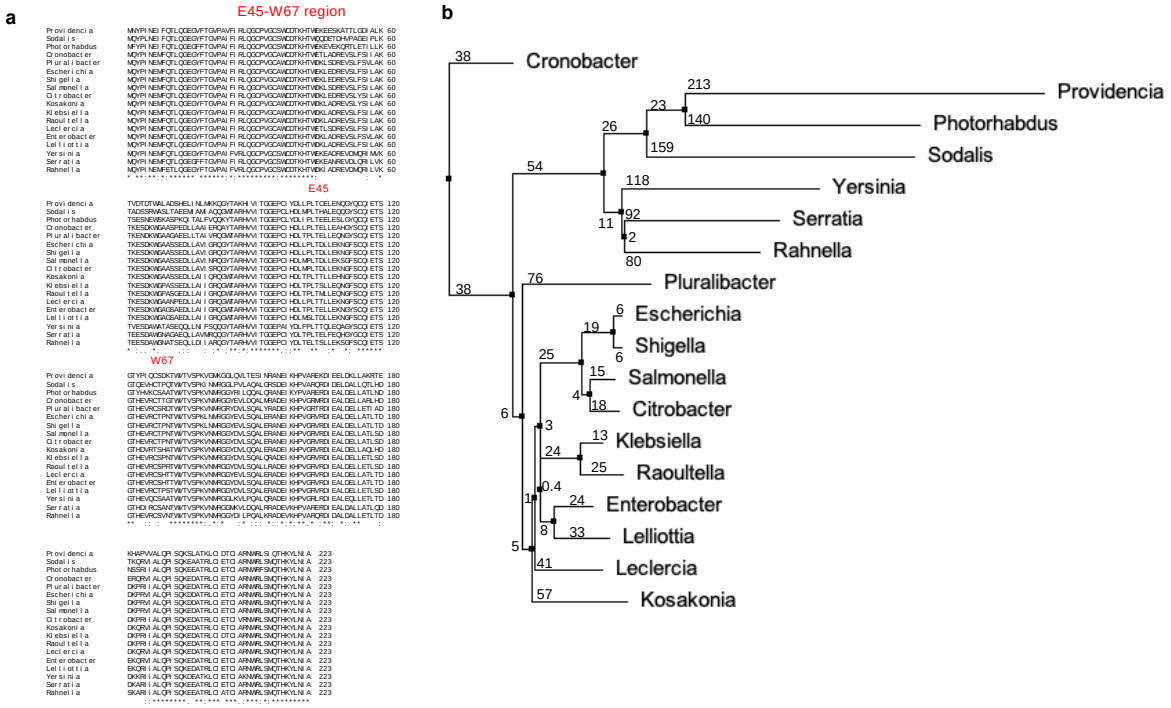

Figure S8. Sequence analysis and phylogeny of selected QueE orthologs from gammaproteobacteria (a) Multiple sequence alignment of 18 QueE orthologs from representative enterobacteria generated using ClustalW. The E45-W67 region is highlighted in red. (b). Phylogenetic tree of the selected QueE sequences estimated by the neighbor-joining method (BLOSUM62) using Jalview[5].

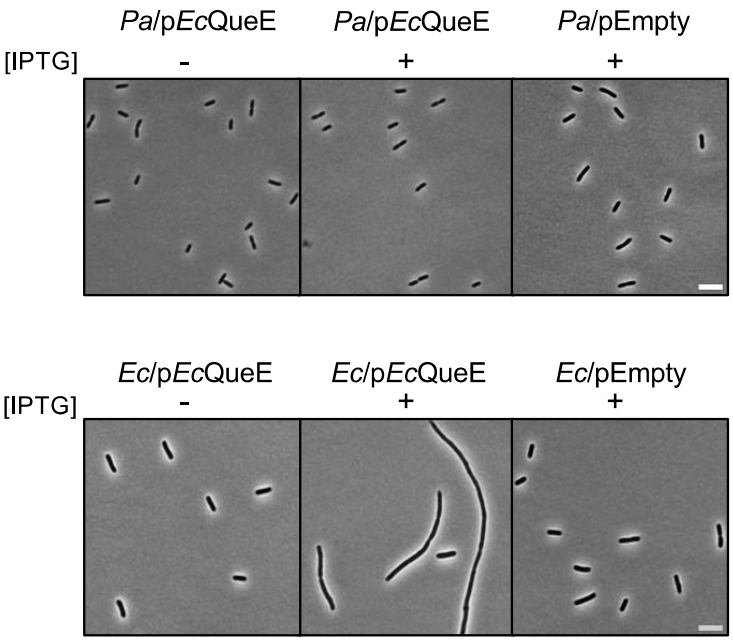

Figure S9. Expression of *Ec*QueE in *P. aeruginosa*. Representative phase-contrast micrographs of *E. coli* and *P. aeruginosa* cells carrying either p*Ec*QueE (pSA157) or pEmpty (pPSV38 shuttle vector) in the presence or absence of IPTG. IPTG levels of 0.5 mM and 2 mM were used for *E. coli* and *P. aeruginosa*, respectively. Scale bar = 5 µm.

References

1. Yadavalli SS, Carey JN, Leibman RS, Chen AI, Stern AM, Roggiani M, et al. Antimicrobial peptides trigger a division block in Escherichia coli through stimulation of a signalling system. Nat Commun. 2016;7: 12340.

2. Bullock WO. XL1-blue : a high efficiency plasmid transforming recA Escherichia coli strain with beta-ga-lactosidase selection. Biotechniques. 1987;5: 376.

3. Galli E, Gerdes K. Spatial resolution of two bacterial cell division proteins: ZapA recruits ZapB to the inner face of the Z-ring. Mol Microbiol. 2010;76: 1514–1526.

4. Amann E, Ochs B, Abel KJ. Tightly regulated tac promoter vectors useful for the expression of unfused and fused proteins in Escherichia coli. Gene. 1988;69: 301–315.

5. Waterhouse AM, Procter JB, Martin D, Clamp M, Barton GJ. Jalview Version 2 - A multiple sequence alignment editor and analysis workbench. Bioinformatics. 2009;25: 1189–1191.